

Endmember Extraction from Hyperspectral Images Using Self-Dictionary Approach with Linear Programming

Tomohiko Mizutani

Abstract—Hyperspectral imaging technology has a wide range of applications, including forest management, mineral resource exploration, and Earth surface monitoring. A key step in utilizing this technology is endmember extraction, which aims to identify the spectral signatures of materials in observed scenes. Theoretical studies suggest that self-dictionary methods using linear programming (LP), known as Hottopixx methods, are effective in extracting endmembers. However, their practical application is hindered by high computational costs, as they require solving LP problems whose size grows quadratically with the number of pixels in the image. As a result, their actual effectiveness remains unclear. To address this issue, we propose an enhanced implementation of Hottopixx designed to reduce computational time and improve endmember extraction performance. We demonstrate its effectiveness through experiments. The results suggest that our implementation enables the application of Hottopixx for endmember extraction from real hyperspectral images and allows us to achieve reasonably high accuracy in estimating endmember signatures.

Index Terms—Hyperspectral imaging, endmember extraction, nonnegative matrix factorization, linear mixing model, pure pixel, self-dictionary, linear programming, column generation method.

I. INTRODUCTION

A hyperspectral camera is an optical instrument used to measure the spectra of materials in a scene. The resulting hyperspectral images (HSIs) typically consist of several hundred spectral bands, enabling detailed analysis of material composition. Endmember extraction from HSIs aims to identify the spectral signatures of materials (i.e., the major components in observed scenes). This process is a key step in utilizing hyperspectral imaging for practical applications. For a comprehensive overview of the latest advancements in hyperspectral image analysis, refer to the tutorial paper [15].

Self-dictionary methods are known as promising approaches for extracting endmembers from HSIs. These methods formulate the task as a sparse optimization problem using the data itself as a dictionary, and then employ convex relaxation techniques to solve it. In 2012, Bittorf et al. [6] developed the Hottopixx method, originally designed for extracting hot topics from documents. This method can be viewed as a self-dictionary approach for the task of extracting endmembers from HSIs. Since the work of Bittorf et al., several authors [16], [19], [28] have refined Hottopixx and examined the

performance of their refinements both theoretically and practically.

Hottopixx methods employ a linear programming (LP) problem, referred to as the Hottopixx model, as a relaxation of the sparse optimization formulation. Typically, these methods involve two main steps: first, compute the optimal solution to the Hottopixx model; second, identify endmembers based on information obtained from the optimal solution. The second step serves as a postprocessing procedure for Hottopixx. In [16], [28], the authors proposed a clustering algorithm for postprocessing, which improves the endmember extraction performance of Hottopixx methods. They provided theoretical evidence to support this approach in their study.

However, the practical application of Hottopixx methods is hindered by high computational costs associated with solving Hottopixx models, as the size of the models grows quadratically with the number of pixels in the HSI. As a result, it is unclear whether these methods are actually effective in extracting endmembers from HSIs. To address this issue, we propose an enhanced implementation of the Hottopixx method of [28]. As summarized below, our approach can significantly reduce computational time and improve the accuracy of the estimated endmember signatures. Therefore, we refer to it as EEHT, an efficient and effective implementation of Hottopixx for the endmember extraction task.

The contributions of this study are summarized as follows.

a) Reducing the computational time of Hottopixx: Solving Hottopixx models is computationally costly, which poses an obstacle to applying them to the endmember extraction task. To remedy this issue, we propose a row and column expansion (RCE) algorithm for solving Hottopixx models efficiently. This algorithm follows the framework of column generation, a classical but powerful technique for solving large-scale LPs.

Many zero elements may exist in the optimal solution of a Hottopixx model. This suggests that Hottopixx models can be solved by breaking them up into smaller subproblems and solving them. We present Theorem 2, which shows that the optimal solution of the full Hottopixx model can be obtained by solving its subproblems. We then develop an RCE algorithm based on this theoretical result. The details are described in Section IV.

b) Enhancing the endmember extraction performance of Hottopixx: The postprocessing step in the Hottopixx method described in [28] conducts data clustering and outputs one element from each cluster. The choice of elements affects the endmember extraction performance of Hottopixx. The meth-

ods used in the previous studies [16], [19], [28] were based on the optimal solutions to Hottopixx models. Alternatively, we propose a method based on the shape of clusters; it computes the centroids of each cluster and chooses elements close to them. This method is simple but effective in enhancing the endmember extraction performance of Hottopixx. We will call it the cluster centroid choice. The details are described in Section V.

c) *Demonstrating the performance of EEHT by experiment:* We developed EEHT by incorporating RCE and the cluster centroid choice. We then experimentally tested its performance on endmember extraction problems. The first experiment (Section VI-A) examined the computational time of RCE. The results show that RCE is faster than the direct method of solving Hottopixx models. The second experiment (Section VI-B) evaluated the endmember extraction performance of EEHT on semi-real HSI datasets. We compared EEHT with six existing methods, including MERIT from [30], which is a method based on a self-dictionary, similar to EEHT. The results show that, in terms of the estimation accuracy of the endmember signatures, the performance of EEHT is comparable to MERIT when the penalty parameter of MERIT is properly adjusted. Finally, we conducted an experimental study (Section VI-C) on hyperspectral unmixing of the Urban HSI dataset. The results show that, compared with the existing methods, EEHT usually provides more accurate estimations of endmember signatures for Urban.

A. Organization of This Paper

This paper is organized as follows. Section II is devoted to the preliminaries. Section III formulates the endmember extraction problem and explains the algorithm of Hottopixx. It also reviews related methods. Section IV and Section V present the details of the RCE and EEHT. Section VI describes the experiments.

II. PRELIMINARIES

A. Notation

$\mathbf{0}$ denotes a vector of all zeros, $\mathbf{1}$ a vector of all ones, O a matrix of all zeros, I the identity matrix, and J a matrix of all ones. $\mathbb{R}_+^{d \times n}$ represents the set of nonnegative matrices.

Let $\mathbf{a} \in \mathbb{R}^d$ and $A \in \mathbb{R}^{d \times n}$. The notation $\mathbf{a}(i)$ indicates the i th entry of \mathbf{a} . Similarly, $A(i, j)$ indicates the (i, j) th entry of A , $A(i, :)$ the i th row, and $A(:, j)$ the j th column. The j th column is also denoted by \mathbf{a}_j . We write $\text{tr}(A)$ for the trace of A . The notation $\text{diag}(\mathbf{a})$ refers to a diagonal matrix of size d containing the elements of \mathbf{a} in the diagonal positions. Let A be a square matrix, i.e., $d = n$. In this case, $\text{diag}(A)$ refers to a vector of size d consisting of the diagonal elements of A .

We use \mathcal{N} to denote $\{1, \dots, n\}$. Let $A = [\mathbf{a}_1, \dots, \mathbf{a}_n] \in \mathbb{R}^{d \times n}$. For $\mathcal{I} \subset \mathcal{N}$, we use $A(\mathcal{I})$ or $[\mathbf{a}_i : i \in \mathcal{I}]$ to denote the submatrix of A indexed by \mathcal{I} in ascending order. Specifically, if $\mathcal{I} = \{i_1, \dots, i_p\}$ with $i_1 < \dots < i_p$, then $A(\mathcal{I}) = [\mathbf{a}_{i_1} : i \in \mathcal{I}] = [\mathbf{a}_{i_1}, \dots, \mathbf{a}_{i_p}]$.

We use $\|\cdot\|$ to denote any norm of a vector or a matrix. In particular, $\|\cdot\|_p$ refers to the L_p -norm of a vector or a matrix, and $\|\cdot\|_F$ the Frobenius norm of a matrix. For $A \in \mathbb{R}^{d \times n}$, we

define $\|A\|_{p,q} = \sum_{i=1}^n \|A(i, :)\|_p^q$ and use $\|A\|_{\text{row},0}$ to denote the number of nonzero rows in A . Moreover, $\langle A, B \rangle$ indicates the inner product of two matrices A and B of the same size, defined by $\langle A, B \rangle = \text{tr}(A^\top B)$.

For $A \in \mathbb{R}^{d \times n}$ (resp. $\mathbf{a} \in \mathbb{R}^d$), we define A^+ (resp. \mathbf{a}^+) to be the matrix (resp. vector) obtained by replacing all negative values of A (resp. \mathbf{a}) with zero. Moreover, we define A^- by $A^- = A^+ - A$. Hence, A^+ and A^- satisfy $A^+, A^- \geq O$ and $A = A^+ - A^-$. The L_1 norm of A can be written using A^+ and A^- as follows:

$$\|A\|_1 = \max_{j=1, \dots, n} \sum_{i=1}^d A^+(i, j) + A^-(i, j). \quad (1)$$

Additionally, for an optimization problems S , we denote the optimal value of S by $\text{opt}(S)$. For a set \mathcal{I} , we use $|\mathcal{I}|$ to denote the number of elements in \mathcal{I} .

B. Duality of LP Problems

As mentioned in Section I, we propose the RCE algorithm for solving Hottopixx models efficiently. This algorithm is founded on the duality of LP problems. For $A \in \mathbb{R}^{d \times n}$, $\mathbf{b} \in \mathbb{R}^d$ and $\mathbf{c} \in \mathbb{R}^n$, consider the primal and dual pair of LP,

$$\begin{aligned} \text{(Primal)} \quad & \min_{\mathbf{x} \in \mathbb{R}^n} \quad \mathbf{c}^\top \mathbf{x} \quad \text{s.t.} \quad A\mathbf{x} = \mathbf{b}, \quad \mathbf{x} \geq \mathbf{0}. \\ \text{(Dual)} \quad & \max_{\mathbf{y} \in \mathbb{R}^d} \quad \mathbf{b}^\top \mathbf{y} \quad \text{s.t.} \quad A^\top \mathbf{y} \leq \mathbf{c}. \end{aligned}$$

- *The duality theorem:* If the primal and dual are feasible, then, there exist optimal solutions \mathbf{x} and \mathbf{y} to the primal and dual and they satisfy $\mathbf{c}^\top \mathbf{x} = \mathbf{b}^\top \mathbf{y}$.
- *Implication of the weak duality theorem:* Let \mathbf{x} and \mathbf{y} be feasible solutions to the primal and dual. If $\mathbf{c}^\top \mathbf{x} = \mathbf{b}^\top \mathbf{y}$, then, \mathbf{x} and \mathbf{y} are optimal solutions to the primal and dual.

For more details, refer to the textbooks [3], [4]. We will use these results to develop RCE.

III. SELF-DICTIONARY APPROACHES FOR SOLVING ENDMEMBER EXTRACTION PROBLEMS

A. Endmember Extraction of HSIs

Suppose that we are given an HSI data for some area consisting of n pixels acquired by a hyperspectral camera with d spectral bands. We represent the HSI as a matrix $A \in \mathbb{R}^{d \times n}$ where the (i, j) th entry of A stores the measurement at the i th band and j th pixel. In this paper, we refer to such a matrix A an *HSI matrix*. The j th column \mathbf{a}_j of A corresponds to the observed spectral signature at the j th pixel.

Let $A = [\mathbf{a}_1, \dots, \mathbf{a}_n] \in \mathbb{R}^{d \times n}$ be an HSI matrix and let us consider a linear mixing model (LMM) for A . Under the LMM, the observed spectral signatures $\mathbf{a}_1, \dots, \mathbf{a}_n$ at each pixel are written as

$$\mathbf{a}_j = \sum_{i=1}^r h_{ij} \mathbf{w}_i + \mathbf{v}_j, \quad j = 1, \dots, n.$$

Here, \mathbf{w}_i satisfies $\mathbf{w}_i \geq \mathbf{0}$ and represents the i th endmember signature; h_{ij} satisfies $\sum_{i=1}^r h_{ij} = 1$, $h_{ij} \geq 0$ and represents the abundance fraction of the i th endmember signature at the

j th pixel; v_j represents noise. The equation above can be expressed in matrix form as

$$A = WH + V \quad (2)$$

by letting $W = [\mathbf{w}_1, \dots, \mathbf{w}_r] \in \mathbb{R}_+^{d \times r}$, $H \in \mathbb{R}_+^{r \times n}$ such that $H(i, j) = h_{ij}$, and $V = [\mathbf{v}_1, \dots, \mathbf{v}_n] \in \mathbb{R}^{d \times n}$. We call W and H the *endmember matrix* and the *abundance matrix* of A , respectively.

Endmember signatures, represented by $\mathbf{w}_1, \dots, \mathbf{w}_r$, are the spectral signatures of certain materials contained in the image scene. The term *endmember* is used for referring to the corresponding material; hence, endmembers are materials contained in the image scene and represent the major components of it.

We will make some assumptions about the HSIs. We say that a pixel is *pure* if it contains a single material corresponding to some endmember. We assume that there is at least one pure pixel for every endmember. This is called the *pure pixel assumption*. Accordingly, the HSI matrix A shown in (2) can be rewritten as

$$A = W[I, \bar{H}]\Pi + V \quad (3)$$

for $W \in \mathbb{R}_+^{d \times r}$, $\bar{H} \in \mathbb{R}_+^{r \times (n-r)}$, $V \in \mathbb{R}^{d \times n}$ and a permutation matrix Π of size n . If A is noiseless, i.e., $V = O$, then, we have $A = W[I, \bar{H}]\Pi$, which implies that all columns of W appear among those of A . Furthermore, we assume that the number of endmembers in an HSI is known in advance. We can now formulate the endmember extraction problem as follows.

Problem 1: Given the HSI matrix A shown in (3) and the number r of endmembers, find r columns of A close to those of the endmember matrix W .

The pure pixel assumption is considered reasonable. Meanwhile, it is difficult to determine the exact number of endmembers in an HSI. Thus, in our experiments we estimate it in the way shown in previous studies. Problem 1 is known to be equivalent to the problem of computing a nonnegative matrix factorization (NMF) under the separability assumption. Arora et al. [2] studied the separable NMF problems from a theoretical point of view. Their results tell us that we can find W from A exactly if A is noiseless; otherwise, if A contains noise V so that the amount of V is smaller than some level, we can find r columns of A close to those of W . Given A as shown in (3), we say that an algorithm for Problem 1 is *robust to noise* if it can find r such columns of A . For further reading on separable NMF, refer to [12], [18].

Once Problem 1 is solved, we can compute the abundance matrix H of A from the estimated endmember signatures. Let \mathcal{I} be the index set of r columns found in the problem. Then, H is the optimal solution to the following convex optimization problem:

$$\min_{X \in \mathbb{R}^{r \times n}} \|A - A(\mathcal{I})X\|_F^2 \quad \text{s.t.} \quad \mathbf{1}^\top X = \mathbf{1}^\top, X \geq O. \quad (4)$$

We need to evaluate the accuracy of the estimated endmember signatures. In this paper, we use the mean-removed spectral angle (MRSA) of two spectral signatures for this evaluation.

For $\mathbf{c} \in \mathbb{R}^d$, we set $\text{ave}(\mathbf{c}) = (\mathbf{1}^\top \mathbf{c}/d) \cdot \mathbf{1} \in \mathbb{R}^d$. For spectral signature vectors $\mathbf{a}, \mathbf{b} \in \mathbb{R}^d$, the MRSA is defined as

$$\text{MRSA}(\mathbf{a}, \mathbf{b}) = \frac{1}{\pi} \arccos \frac{(\mathbf{a} - \text{ave}(\mathbf{a}))^\top (\mathbf{b} - \text{ave}(\mathbf{b}))}{\|\mathbf{a} - \text{ave}(\mathbf{a})\|_2 \|\mathbf{b} - \text{ave}(\mathbf{b})\|_2},$$

which takes values in the interval from 0 to 1. A smaller MRSA value for \mathbf{a} and \mathbf{b} means that \mathbf{a} is more similar to \mathbf{b} .

B. Hottopixx Methods

Dictionary learning methods are often used for extracting endmembers from HSIs. Let us consider the input matrix A of Problem 1 as a dictionary and the columns of A as the atoms of the dictionary. The problem can thus be restated as one of choosing r atoms from the dictionary to achieve a good approximation of the dictionary by means of nonnegative linear combinations of the chosen atoms. Since the input matrix A itself is used as a dictionary, it is referred to as a *self-dictionary*. It should be noted that the pure pixels assumption is made for HSIs in Problem 1; thus we can use A as a dictionary. In cases where this assumption does not hold, see Remark 1.

From the perspective of dictionary learning, let us formulate Problem 1 as a sparse optimization problem,

$$\min_{X \in \mathbb{R}^{n \times n}} \|A - AX\| \quad (5a)$$

$$\text{s.t.} \quad \|X\|_{\text{row},0} = r, \mathbf{1}^\top X = \mathbf{1}^\top, X \geq O. \quad (5b)$$

This problem is difficult to solve since it includes the combinatorial constraint $\|X\|_{\text{row},0} = r$. Hottopixx methods were initially proposed by Bittorf et al. [6] in 2012 in the context of topic modeling. Subsequently, several refinements [16], [19], [28] have been developed. These methods are based on the LP relaxation of problem (5).

In this paper, we propose an implementation of the Hottopixx method that was proposed in [28]. To this end, we review the details of the Hottopixx method below. For a given A and r in Problem 1, the first step of the Hottopixx method involves constructing an optimization problem,

$$\text{H:} \quad \min_{X \in \mathbb{R}^{n \times n}} \|A - AX\|_1 \quad \text{s.t.} \quad X \in \mathcal{F}.$$

The feasible region \mathcal{F} is defined by

$$\sum_{i=1}^n X(i, i) = r, \\ 0 \leq X(i, j) \leq X(i, i) \leq 1, \quad i, j = 1, \dots, n.$$

In this paper, we call H the *Hottopixx model*, although it differs from the original Hottopixx model proposed by Bittorf et al. [6]. As shown in Section IV-B, H can be reduced to an LP problem. The previous study [28] directly solved this LP using a CPLEX solver. The constraints of H relax the constraint $\|X\|_{\text{row},0} = r$ of problem (5). However, it is possible for many rows of the optimal solution X in H to be zero, since the constraints of H imply that the i th row of X is zero if $X(i, i) = 0$ and many of $X(1, 1), \dots, X(n, n)$ could be zero.

Problem (5) includes the sum-to-one constraint $\mathbf{1}^\top X = \mathbf{1}^\top$, but we exclude it from H, as the original Hottopixx model does

not include it. As described in Remark 1 of [16], theoretical studies suggest that the endmember extraction performance of Hottopixx methods can be further enhanced by incorporating the sum-to-one constraint into H.

The second step involves choosing r columns of A using the optimal solution X of H. A simple way of doing so is to find a set \mathcal{I} of r indices corresponding to the r largest elements of $\text{diag}(X)$ and, then, output columns \mathbf{a}_i with $i \in \mathcal{I}$. Theorem 3.1 of [28] ensures that the algorithm is robust to noise. However, the theorem is invalid and does not hold in a case where there are overlaps of pure pixels in the HSIs. To cope with this issue, we use a clustering technique. Algorithm 1 describes each step of Hottopixx with postprocessing [28]. A cluster \mathcal{S}_ℓ in the algorithm refers to a subset of the column index set \mathcal{N} of A . Due to page limitations, a detailed description of how to construct clusters is provided in Appendix B.

Algorithm 1 Hottopixx with postprocessing (Algorithm 5.1 of [28])

Input: $A = [\mathbf{a}_1, \dots, \mathbf{a}_n] \in \mathbb{R}^{d \times n}$ and a positive integer r .

Output: r columns of A .

- 1: Compute the optimal solution X of H.
- 2: Set $\mathbf{p}_1 = \text{diag}(X)$, $\mathcal{I} = \emptyset$ and $\ell = 1$. Perform the following procedure.
 - 2-1: Construct a cluster \mathcal{S}_ℓ using \mathbf{p}_ℓ ; see Appendix B for the details.
 - 2-2: Choose one element from \mathcal{S}_ℓ and add it to \mathcal{I} . Increase ℓ by 1.
 - 2-3: If $\ell = r$, return \mathbf{a}_i with $i \in \mathcal{I}$ and terminate; otherwise, construct \mathbf{p}_ℓ as

$$\mathbf{p}_\ell(u) = \begin{cases} 0 & \text{if } u \in \mathcal{S}_1 \cup \dots \cup \mathcal{S}_{\ell-1}, \\ \mathbf{p}_1(u) & \text{otherwise,} \end{cases}$$

and go to step 2-1.

Algorithm 1 has an advantage over other algorithms [6], [16], [19] in that it does not require us to specify the noise level involved in A as input. Theorem 3.2 of [28] ensures that Algorithm 1 is robust to noise. Even if there are overlaps among pure pixels in the HSI, the theorem remains valid and the algorithm is robust to noise. In most cases, there are a number of pixels in the HSIs that are close to pure pixels. Specifically, we will see this feature in the Urban dataset in Section VI-C. Hence, when solving Problem 1, we should use the postprocessing procedure described in step 2 of Algorithm 1.

Remark 1: If the pure pixel assumption does not hold for HSIs, the input matrix A of Problem 1 no longer serves as a dictionary. In such cases, since there are libraries containing numerous spectral signatures of materials, as proposed in [23]–[25] it is feasible to construct a dictionary by collecting samples from these libraries.

C. Related Methods

So far, many methods have been proposed for addressing Problem 1, as detailed in the survey papers [5], [26] and

the textbook [18]. These methods can be categorized into two groups: convex optimization-based methods and greedy methods. Hereinafter, we will use the term “convex method” as a shorthand to refer to the convex optimization-based method. Convex methods are robust to noise but computationally expensive, whereas greedy methods are faster but less robust. Hottopixx is an example of a convex method.

1) *Convex Methods:* As mentioned earlier, Problem 1 can be formulated as a sparse optimization problem. However, directly solving sparse optimization problems is computationally intractable. Thus, we instead solve their convex relaxation problems. A typical algorithm for convex methods involves computing the optimal solution to the convex relaxation problem and subsequently extracting r columns of A using this optimal solution.

Our approach is closely related to FGNSR, proposed by Gillis and Luce [20], and MERIT, proposed by Nguyen, Fu and Wu [30], both of which are convex methods using self-dictionaries. Here, let us recall problem (5), which is the sparse optimization formulation for Problem 1. FGNSR and MERIT solve its convex relaxation as follows:

$$\min_{X \in \mathbb{R}^{n \times n}} \frac{1}{2} \|A - AX\|_F^2 + \lambda \cdot \Phi(X) \quad \text{s.t. } X \in \mathcal{G} \quad (6)$$

for a penalty parameter $\lambda \geq 0$, where Φ is the regularization term and \mathcal{G} is the feasible region. Here, Φ is designed to minimize the number of nonzero rows in X .

FGNSR uses $\Phi(X) = \tau^\top \text{diag}(X)$, where $\tau \in \mathbb{R}^n$ is close to $\mathbf{1}$. It uses \mathcal{G} defined by

$$\begin{aligned} X(i, i) &\leq 1, & i &= 1, \dots, n, \\ c_i X(i, j) &\leq c_j X(i, i), & i, j &= 1, \dots, n, \\ X &\geq O \end{aligned}$$

where $c_i = \|A(:, i)\|_1$. Problem (6) with Φ and \mathcal{G} as described above is closely related to the original Hottopixx model by Bittorf et al. [6]. Gillis and Luce [20] showed that the projection of a matrix onto \mathcal{G} can be computed in $O(n^2 \log n)$. Taking that into account it, they developed a first-order method equipped with Nesterov’s acceleration to solve these problems.

MERIT uses $\Phi(X) = \sum_{i=1}^n \phi_\mu(X(i, :))$, where

$$\phi_\mu(\mathbf{x}) = \mu \log \left(\frac{1}{n} \sum_{i=1}^n \exp \frac{x_i}{\mu} \right) \quad (7)$$

for $\mathbf{x} = [x_1, \dots, x_n]^\top \in \mathbb{R}^n$ and a parameter $\mu > 0$. It uses \mathcal{G} defined by $\mathbf{1}^\top X = \mathbf{1}^\top$ and $X \geq O$, referred to as the simplex constraint. The function $\Phi(X)$ serves as a smooth approximation of $\|X\|_{\infty, 1}$, as the relation $\|\mathbf{x}\|_\infty - \mu \log n \leq \phi_\mu(\mathbf{x}) \leq \|\mathbf{x}\|_\infty$ holds. Accordingly, minimizing $\Phi(X)$ causes many rows of X to be zero when μ is small. Nguyen, Fu and Wu [30] proposed to solve such problems with the Frank-Wolfe method. They also examined the theoretical performance of MERIT in their study.

Convex methods for solving Problem 1 and related problems can be found in the papers by Elhamifar, Sapiro and Vidal [10] and by Esser et al. [11], both published in 2012. Fu and Ma [13] analyzed the performance of convex method based on problem (6) with $\Phi(X) = \|X\|_{\infty, q}$ for $0 < q \leq 1$ and with

\mathcal{G} defined by the simplex constraint. Fu, Sidiropoulos and Ma [14] applied convex optimization approaches to power spectral separation.

2) *Greedy Methods*: Greedy methods choose the columns of the HSI matrix one by one on the basis of certain criteria. One of the most popular greedy methods for solving Problem 1 is SPA, which dates back to the work of Araújo et al. [1] in 2001. Subsequently, Gillis and Vavasis [21] gave a theoretical justification for the robustness of SPA to noise. SPA recursively chooses the columns of the input matrix. For a column chosen in the previous iteration, it projects columns onto the orthogonal complement of the chosen column and then chooses one with the maximum L_2 norm. To enhance the robustness of SPA to noise, Gillis and Vavasis [22] developed PSPA, which is SPA with preconditioning, and Mizutani [27] ER, which is SPA with a preprocessing. Both preconditioning and preprocessing use singular value decomposition (SVD) based dimensionality reduction and minimum volume ellipsoids. Gillis [17] proposed SNPA, which is similar to that of SPA but it uses a projection onto the convex hull of the origin and previously chosen columns. Nascimento and Bioucas-Dias [29] proposed VCA, which applies an SVD-based dimensionality reduction to the input matrix, and then, runs the same algorithm as SPA except for the criterion for choosing columns. Other popular methods in the remote sensing community include PPI [7], N-FINDR [31], and AVMAX and SVMAX [9].

IV. SOLVING HOTTOPIXX MODELS EFFICIENTLY

A. Algorithm Outline

In Section IV-B, we show that H can be reduced to an LP with $O(n^2)$ variables and $O(n^2)$ constraints for HSI matrices $A \in \mathbb{R}^{d \times n}$ with $d \leq n$. Accordingly, when n is large, directly solving the LP, as in the previous study [28], becomes computationally challenging. To remedy this computational issue, we develop the RCE algorithm for solving H efficiently based on the framework of column generation, which is known as a classical but powerful technique for solving large-scale LPs; see, for instance, the textbook [4] for details on column generation methods. The algorithm is based on the observation that there may be many zero rows in the optimal solution of H. We can significantly reduce the size of H by exploiting the sparsity of the optimal solution.

Let \mathcal{L} and \mathcal{M} be the subsets of \mathcal{N} . Hereinafter, we will use ℓ and m to denote $|\mathcal{L}|$ and $|\mathcal{M}|$, respectively. RCE uses a subproblem of H with a variable $X \in \mathbb{R}^{\ell \times m}$. The feasible region $\mathcal{F}(\ell, m)$ is defined by

$$\begin{aligned} \sum_{i=1}^{\ell} X(i, i) &= r, \\ 0 \leq X(i, j) \leq X(i, i) \leq 1, \quad &i = 1, \dots, \ell, \quad j = 1, \dots, m. \end{aligned}$$

Here, we consider the following subproblem:

$$H' : \min_{X \in \mathbb{R}^{\ell \times \ell}} \|A(\mathcal{L}) - A(\mathcal{L})X\|_1 \quad \text{s.t.} \quad X \in \mathcal{F}(\ell, \ell).$$

H' has fewer variables and constraints than the original problem H. Hence, solving H' is computationally cheaper than

solving H. We show in Theorem 2 the conditions under which the optimal solution of H' yields the optimal solution of H. Based on this theorem, we design an algorithm for solving H efficiently, which can be outlined as follows: solve H' and verify the conditions; if the conditions are not satisfied, update \mathcal{L} by adding some elements in $\mathcal{N} \setminus \mathcal{L}$ to \mathcal{L} and solve H' again. We call this algorithm ‘‘row and column expansion’’, RCE, since it starts from the optimal solution X of H' , and then expands the rows and the columns of X step-by-step.

B. Subproblem of H

Here, we formally describe the subproblem of H. For given subsets \mathcal{L} and \mathcal{M} of \mathcal{N} satisfying $\mathcal{L} \subset \mathcal{M}$, choose a permutation matrix $\Pi \in \mathbb{R}^{m \times m}$ such that

$$A(\mathcal{M})\Pi = [A(\mathcal{L}), A(\mathcal{M} \setminus \mathcal{L})].$$

Then, construct the subproblem,

$$\begin{aligned} H(\mathcal{L}, \mathcal{M}) : \quad &\min_{X \in \mathbb{R}^{\ell \times m}} \|A(\mathcal{M})\Pi - A(\mathcal{L})X\|_1 \\ &\text{s.t.} \quad X \in \mathcal{F}(\ell, m). \end{aligned}$$

The permutation matrix Π is chosen to be the identity matrix when $\mathcal{L} = \mathcal{M}$. Hence, H coincides with $H(\mathcal{N}, \mathcal{N})$. We can reduce $H(\mathcal{L}, \mathcal{M})$ to the following LP problem,

$$\begin{aligned} P(\mathcal{L}, \mathcal{M}) : \quad &\min \quad u \\ &\text{s.t.} \quad A(\mathcal{M})\Pi - A(\mathcal{L})X = F - G, \\ &\quad \sum_{i=1}^d F(i, j) + G(i, j) \leq u, \quad j = 1, \dots, m, \\ &\quad F \geq O, \quad G \geq O, \quad X \in \mathcal{F}(\ell, m). \end{aligned}$$

Here, $(X, F, G, u) \in \mathbb{R}^{\ell \times m} \times \mathbb{R}^{d \times m} \times \mathbb{R}^{d \times m} \times \mathbb{R}$ is the variable. We show in Theorem 1 that solving $P(\mathcal{L}, \mathcal{M})$ is equivalent to solving $H(\mathcal{L}, \mathcal{M})$. We add slack variables to the inequality constraints and convert $P(\mathcal{L}, \mathcal{M})$ to a standard form LP. Then, the dual problem becomes

$$\begin{aligned} D(\mathcal{L}, \mathcal{M}) : \quad &\max \quad \langle A(\mathcal{M})\Pi, Y \rangle + rv - \mathbf{1}^\top \mathbf{t} \\ &\text{s.t.} \quad A(\mathcal{L})^\top Y + [vI, O] - [\text{diag}(\mathbf{t}), O] \\ &\quad - Z^\top + [\text{diag}(Z^\top \mathbf{1}), O] \leq O, \\ &\quad - J \cdot \text{diag}(\mathbf{s}) \leq Y \leq J \cdot \text{diag}(\mathbf{s}), \\ &\quad \mathbf{1}^\top \mathbf{s} \leq 1, \\ &\quad \mathbf{s} \geq \mathbf{0}, \quad \mathbf{t} \geq \mathbf{0}, \quad Z \geq O \end{aligned}$$

Here, $(Y, Z, \mathbf{s}, \mathbf{t}, v) \in \mathbb{R}^{d \times m} \times \mathbb{R}^{m \times \ell} \times \mathbb{R}^m \times \mathbb{R}^\ell \times \mathbb{R}$ is the variable.

It is obvious that there exist feasible solutions to $P(\mathcal{L}, \mathcal{M})$ and $D(\mathcal{L}, \mathcal{M})$. Hence, the duality theorem, which we reviewed in Section II-B, holds and ensures that there are optimal solutions to $P(\mathcal{L}, \mathcal{M})$ and $D(\mathcal{L}, \mathcal{M})$ and that $\text{opt}(P(\mathcal{L}, \mathcal{M})) = \text{opt}(D(\mathcal{L}, \mathcal{M}))$ holds.

Theorem 1: For any subsets \mathcal{L} and \mathcal{M} of \mathcal{N} satisfying $r \leq \ell \leq m$, the following hold.

- (i) $\text{opt}(P(\mathcal{L}, \mathcal{M})) = \text{opt}(D(\mathcal{L}, \mathcal{M})) = \text{opt}(H(\mathcal{L}, \mathcal{M}))$.
- (ii) If (X^*, F^*, G^*, u^*) is the optimal solution of $P(\mathcal{L}, \mathcal{M})$, then X^* is the optimal solution of $H(\mathcal{L}, \mathcal{M})$.

- (iii) If X^* is the optimal solution of $H(\mathcal{L}, \mathcal{M})$, then, $(X^*, R^+, R^-, \|R\|_1)$ for $R = A\Pi - A(\mathcal{L})X^*$ is the optimal solution of $P(\mathcal{L}, \mathcal{M})$.

The proof is provided in Appendix C.

C. Description of the RCE Algorithm

The optimal solution of H can be obtained by solving $P(\mathcal{L}, \mathcal{L})$ and $D(\mathcal{L}, \mathcal{L})$ under certain conditions. Theorem 2 below is the formal statement of this assertion. To describe it, we introduce an auxiliary problem: for a given matrix $X^* \in \mathbb{R}^{\ell \times \ell}$, construct

$$\begin{aligned} R_j(\mathcal{L}, X^*) : \quad & \min_{\gamma_j \in \mathbb{R}^\ell} \quad \|\mathbf{a}_j - A(\mathcal{L})\gamma_j\|_1 \\ & \text{s.t.} \quad \mathbf{0} \leq \gamma_j \leq \text{diag}(X^*) \end{aligned}$$

for $j \in \mathcal{N} \setminus \mathcal{L}$.

Theorem 2: Let $\mathcal{L} \subset \mathcal{N}$. Let $\alpha^* = (X^*, F^*, G^*, u^*)$ be the optimal solution of $P(\mathcal{L}, \mathcal{L})$ and $\beta^* = (Y^*, Z^*, \mathbf{s}^*, \mathbf{t}^*, v^*)$ be the optimal solution of $D(\mathcal{L}, \mathcal{L})$. Consider the following conditions regarding α^* and β^* .

(C1) X^* of α^* satisfies

$$\text{opt}(R_j(\mathcal{L}, X^*)) \leq \text{opt}(P(\mathcal{L}, \mathcal{L}))$$

for every $j \in \mathcal{N} \setminus \mathcal{L}$.

(C2) Y^* and v^* of β^* satisfy

$$v^* + \mathbf{1}^\top ((Y^*)^\top \mathbf{a}_j)^+ \leq 0$$

for every $j \in \mathcal{N} \setminus \mathcal{L}$.

The following hold.

- (i) Assume that condition (C1) holds. Let $\Gamma^* = [\gamma_j^* : j \in \mathcal{N} \setminus \mathcal{L}]$ for the optimal solution γ_j^* of $R_j(\mathcal{L}, X^*)$. Then,
 - $\text{opt}(H(\mathcal{L}, \mathcal{L})) = \text{opt}(H(\mathcal{L}, \mathcal{N}))$, and
 - the matrix $[X^*, \Gamma^*]$ is the optimal solution of $H(\mathcal{L}, \mathcal{N})$.
- (ii) Assume that conditions (C1) and (C2) hold. Let $\Gamma^* = [\gamma_j^* : j \in \mathcal{N} \setminus \mathcal{L}]$ for the optimal solution γ_j^* of $R_j(\mathcal{L}, X^*)$, and let Π be a permutation matrix of size n such that $A\Pi = [A(\mathcal{L}), A(\mathcal{N} \setminus \mathcal{L})]$. Then,
 - $\text{opt}(H(\mathcal{L}, \mathcal{L})) = \text{opt}(H(\mathcal{N}, \mathcal{N}))$, and
 - the matrix

$$\Pi \begin{bmatrix} X^* & \Gamma^* \\ \mathbf{0} & \mathbf{0} \end{bmatrix} \Pi^\top$$

is the optimal solution of $H(\mathcal{N}, \mathcal{N})$.

The proof is provided in Appendix A. Note that $((Y^*)^\top \mathbf{a}_j)^+$ in condition (C2) is equivalent to \mathbf{b}_j^+ for $\mathbf{b}_j = (Y^*)^\top \mathbf{a}_j$. One might be concerned that condition (C2) rarely holds; i.e., it will not hold if v^* takes a positive number. However, this concern is alleviated by Lemma 1, which ensures that v^* always takes a nonpositive number.

Lemma 1: Let $(Y^*, Z^*, \mathbf{s}^*, \mathbf{t}^*, v^*)$ be the optimal solution of $D(\mathcal{L}, \mathcal{L})$. If \mathcal{L} is chosen to satisfy $\ell \geq r$, then $v^* \leq 0$.

The proof is provided in Appendix D. Algorithm 2 below is the RCE algorithm for computing the optimal solution of H.

Algorithm 2 RCE : Row and column expansion algorithm for computing the optimal solution of H

Input: $A \in \mathbb{R}^{d \times n}$ and a positive integer r .

Output: $X \in \mathbb{R}^{n \times n}$.

- 1: Choose $\mathcal{L} \subset \mathcal{N}$ satisfying $r \leq \ell$.
- 2: Repeat the following procedure until the stopping condition at step 2-3 is satisfied.

2-1: Compute the optimal solution (X^*, F^*, G^*, u^*) of $P(\mathcal{L}, \mathcal{L})$, and the optimal solution $(Y^*, Z^*, \mathbf{s}^*, \mathbf{t}^*, v^*)$ of $D(\mathcal{L}, \mathcal{L})$.

2-2: Compute the optimal solution γ_j of $R_j(\mathcal{L}, X^*)$ for every $j \in \mathcal{N} \setminus \mathcal{L}$.

2-3: If

$$\text{opt}(R_j(\mathcal{L}, X^*)) \leq \text{opt}(P(\mathcal{L}, \mathcal{L}))$$

for every $j \in \mathcal{N} \setminus \mathcal{L}$, go to step 3; otherwise, update \mathcal{L} by

$$\mathcal{L} \cup \{j \in \mathcal{N} \setminus \mathcal{L} \mid \text{opt}(R_j(\mathcal{L}, X^*)) > \text{opt}(P(\mathcal{L}, \mathcal{L}))\},$$

and go back to step 2-1.

3: If

$$v^* + \mathbf{1}^\top ((Y^*)^\top \mathbf{a}_j)^+ \leq 0$$

for every $j \in \mathcal{N} \setminus \mathcal{L}$, then construct the matrix,

$$X = \Pi \begin{bmatrix} X^* & \Gamma^* \\ \mathbf{0} & \mathbf{0} \end{bmatrix} \Pi^\top \in \mathbb{R}^{n \times n}$$

for $\Gamma^* = [\gamma_j^* : j \in \mathcal{N} \setminus \mathcal{L}]$ and a permutation matrix Π such that $A\Pi = [A(\mathcal{L}), A(\mathcal{N} \setminus \mathcal{L})]$, and return the result; otherwise, update \mathcal{L} by

$$\mathcal{L} \cup \{j \in \mathcal{N} \setminus \mathcal{L} \mid v^* + \mathbf{1}^\top ((Y^*)^\top \mathbf{a}_j)^+ > 0\},$$

and go back to step 2.

V. DETAILED DESCRIPTION OF EEHT

This section provides a detailed explanation of EEHT, in which RCE is a key component, as well as a summary of the overall algorithm.

a) Preprocessing: Before running RCE, we apply a dimensionality reduction technique to the input matrix. For a given $A \in \mathbb{R}^{d \times n}$ and a positive integer r as input, we compute the top- r truncated SVD,

$$A_r = U_r \Sigma_r V_r^\top,$$

of A . Here, $\Sigma_r \in \mathbb{R}^{r \times r}$ is diagonal so that the top- r singular values $\sigma_1, \dots, \sigma_r$ of A are in the diagonal positions and the columns of $U_r \in \mathbb{R}^{d \times r}$ (resp. $V_r \in \mathbb{R}^{n \times r}$) are the left-singular (resp. right-singular) vectors of A corresponding to $\sigma_1, \dots, \sigma_r$. Then, we construct a size-reduced matrix $A' = \Sigma_r V_r^\top \in \mathbb{R}^{r \times n}$ of A and run RCE on input (A', r) . It should be noted that, if A is an HSI matrix of size $d \times n$ with r endmembers, as shown in (3), then its size-reduced matrix A' is also an HSI matrix, written as $A' = W'[I, \bar{H}]\Pi + V'$ for $W' \in \mathbb{R}^{r \times r}$ and $V' \in \mathbb{R}^{r \times n}$.

b) *Step 2-2 of Algorithm 1*: In theory, we are allowed to choose any one of the elements in a cluster \mathcal{S}_ℓ at step 2-2 of Algorithm 1. Indeed, Theorem 3.2 of [28] ensures that Algorithm 1 is robust to noise, and this result holds no matter how we choose an element from \mathcal{S}_ℓ at step 2-2. Yet, in practice, the method of choice affects its robustness to noise. For that reason, we employ two methods of choice in step 2-2 of Algorithm 1. The first one, called the *max-point choice*, chooses an element $u \in \mathcal{S}_\ell$ with the highest score according to the point list \mathbf{p}_ℓ :

$$u = \arg \max_{u \in \mathcal{S}_\ell} \mathbf{p}_\ell(u). \quad (8)$$

The max-point choice is not new; it was used in [16], [19], [28] in their postprocessing for Hottopixx. The second one, called the *cluster centroid choice*, defines the centroid \mathbf{c}_ℓ of a cluster \mathcal{S}_ℓ by

$$\mathbf{c}_\ell = \frac{1}{|\mathcal{S}_\ell|} \sum_{u \in \mathcal{S}_\ell} \mathbf{a}_u$$

and then chooses an element $u \in \mathcal{S}_\ell$ such that \mathbf{a}_u is closest to \mathbf{c}_ℓ in terms of MRSA:

$$u = \arg \min_{u \in \mathcal{S}_\ell} \text{MRSA}(\mathbf{c}_\ell, \mathbf{a}_u). \quad (9)$$

The cluster centroid choice is our proposal.

c) *Step 1 of RCE*: The initial choice of \mathcal{L} at step 1 of RCE affects scaling up of the size of \mathcal{L} during the iterations. If the initial choice of \mathcal{L} covers many column indices of A corresponding to pure pixels, we can expect that the increase in the size of \mathcal{L} will be inhibited. We use SPA [1], [21] for this purpose. SPA is fast and the accuracy of its output is reasonable.

Algorithm 3 describes our procedure for constructing an initial set \mathcal{L} . Step 1 uses SPA to find columns $\mathbf{a}_{\ell_1}, \dots, \mathbf{a}_{\ell_r}$ of A that are expected to be close to pure pixels. Step 2 finds the top- ζ nearest neighbors to each $\mathbf{a}_{\ell_1}, \dots, \mathbf{a}_{\ell_r}$ and constructs a set \mathcal{L}_{NN} of their indices. Step 3 chooses η extra elements from the complement of \mathcal{L}_{NN} and constructs a set \mathcal{L}_{EX} of the extras. Step 4 takes the union of \mathcal{L}_{NN} and \mathcal{L}_{EX} and returns it as \mathcal{L} .

Algorithm 4 is the overall procedure of EEHT.

VI. EXPERIMENTS

We conducted experiments to assess the efficiency and effectiveness of EEHT on Problem 1. For the experiments, we coded EEHT in MATLAB. Here, step 2 of EEHT runs RCE whose step 2-1 needs to solve LP problems $P(\mathcal{L}, \mathcal{L})$ and $D(\mathcal{L}, \mathcal{L})$. We employed CPLEX for solving these LP problems. The MATLAB function `cplexlp` is available in the CPLEX package and it enables us to run CPLEX in the MATLAB environment. Applying the `cplexlp` function to an LP returns both the optimal solutions for the LP and its dual. Our code used `cplexlp` for $D(\mathcal{L}, \mathcal{L})$ in order to obtain optimal solutions to both $P(\mathcal{L}, \mathcal{L})$ and $D(\mathcal{L}, \mathcal{L})$. In what follows, EEHT with method A (resp. B, C) chosen at step 3 is referred to as EEHT-A (resp. -B, -C).

We used MRSA to assess the endmember extraction performance. Let $\mathbf{w}_1^{\text{ref}}, \dots, \mathbf{w}_r^{\text{ref}}$ be reference signatures and

Algorithm 3 Construct an initial index set \mathcal{L}

Input: $A \in \mathbb{R}^{d \times n}$ and positive integers r, ζ and η .

Output: $\mathcal{L} \subset \mathcal{N}$.

- 1: Perform SPA on input (A, r) . Let $\mathbf{a}_{\ell_1}, \dots, \mathbf{a}_{\ell_r}$ be the columns of A output by it.
 - 2: Set $\mathcal{L}_{\text{NN}} = \emptyset$. Perform the following procedure for $i = 1, \dots, r$.
 - 2-1: Sort columns $\mathbf{a}_1, \dots, \mathbf{a}_n$ of A by their distance to \mathbf{a}_{ℓ_i} in ascending order so that

$$\|\mathbf{a}_{\ell_i} - \mathbf{a}_{u_1}\|_2 \leq \dots \leq \|\mathbf{a}_{\ell_i} - \mathbf{a}_{u_n}\|_2$$
 where $\{u_1, \dots, u_n\} = \mathcal{N}$.
 - 2-2: Update \mathcal{L}_{NN} by $\mathcal{L}_{\text{NN}} \cup \{u_1, \dots, u_\zeta\}$.
 - 3: Choose η arbitrary elements from $\mathcal{N} \setminus \mathcal{L}_{\text{NN}}$, and construct a set \mathcal{L}_{EX} of them.
 - 4: Set $\mathcal{L} = \mathcal{L}_{\text{NN}} \cup \mathcal{L}_{\text{EX}}$ and return \mathcal{L} .
-

Algorithm 4 EEHT: Efficient and effective implementation of Hottopixx

Input: $A \in \mathbb{R}^{d \times n}$ and positive integers r, ζ , and η .

Output: r columns of A .

- 1: Compute the top- r truncated SVD $A_r = U_r \Sigma_r V_r^\top$ and construct a size-reduced matrix $A' = \Sigma_r V_r^\top$.
 - 2: Run RCE on (A', r) and obtain the output X , where step 1 runs Algorithm 3 on (A', r, ζ, η) .
 - 3: Construct an index set \mathcal{I} by performing one of the following methods A-C and return \mathbf{a}_i with $i \in \mathcal{I}$.
 - A. Find a set \mathcal{I} of r indices corresponding to the r largest elements of $\text{diag}(X)$, and return \mathbf{a}_i with $i \in \mathcal{I}$.
 - B. Run step 2 of Algorithm 1 where step 2-2 adopts the max-point choice of (8).
 - C. Run step 2 of Algorithm 1 where step 2-2 adopts the cluster centroid choice of (9).
-

$\mathbf{a}_{i_1}, \dots, \mathbf{a}_{i_r}$ be the r columns of A returned by the algorithm. We computed a permutation σ of size r such that

$$\min_{\sigma} \sum_{j=1}^r \text{MRSA}(\mathbf{a}_{i_j}, \mathbf{w}_{\sigma(j)}^{\text{ref}}).$$

Note that the minimum is taken over all permutations σ of size r . We then evaluated the MRSA values between the estimated endmember signatures and the reference ones

$$\text{MRSA}(\mathbf{a}_{i_j}, \mathbf{w}_{\sigma(j)}^{\text{ref}}) \text{ for } j = 1, \dots, r \quad (10)$$

and their average,

$$\frac{1}{r} \sum_{j=1}^r \text{MRSA}(\mathbf{a}_{i_j}, \mathbf{w}_{\sigma(j)}^{\text{ref}}). \quad (11)$$

The experiments were done in MATLAB on dual Intel Xeon Gold 6336Y processors with 256 GB of memory.

A. Computational Efficiency

RCE is a key component of EEHT in solving Hottopixx models efficiently. We thus examined the computational time

of RCE on synthetic datasets. The datasets contained HSI matrices $A = W[I, \bar{H}] + V$ with r endmembers that were generated by the following procedure:

- *As for W :* Draw the entries of W from a uniform distribution on the interval $[0, 1]$, and replace them with their absolute values. Finally, normalize the columns of W to have a unit L_1 norm.
- *As for \bar{H} :* Draw the columns of \bar{H} from a Dirichlet distribution with r parameters that are uniformly distributed in the interval $[0, 1]$.
- *As for V :* Draw the entries of V from a standard normal distribution, and normalize V such that $\nu = \|V\|_1$ for a noise intensity level ν specified in advance.

We chose ten equally spaced points between 0 and 1 and set them as noise intensity levels ν . One dataset contained ten HSI matrices $A = W[I, \bar{H}] + V$ of size $50 \times n$ with $r = 10$ satisfying $\nu = \|V\|_1$ for each ν . We set n from 500 to 2500 in 500 increments and, thus, constructed five datasets in total.

We examined four methods, RCE-SR, RCE-DIR, CPLEX-SR, and CPLEX-DIR. Here, RCE-DIR and CPLEX-DIR solved the Hottopixx models H for the original matrices A , while RCE-SR and CPLEX-SR solved theirs for size-reduced matrices A' obtained from the top- r truncated SVD of A . The details are as follows.

- **RCE-SR** constructed a size-reduced matrix A' of A and then applied RCE to A' , where step 1 runs Algorithm 3 with $(\zeta, \eta) = (10, 100)$.
- **RCE-DIR** directly applied RCE to A , where step 1 runs Algorithm 3 with $(\zeta, \eta) = (10, 100)$.
- **CPLEX-SR** constructed a size-reduced matrix A' of A and used `cplexlp` to solve the LP problem $P(\mathcal{N}, \mathcal{N})$ for A' .
- **CPLEX-DIR** directly used `cplexlp` to solve the LP problem $P(\mathcal{N}, \mathcal{N})$ for A .

We compared RCE-SR and -DIR with CPLEX-SR and -DIR, since the Hottopixx methods in [16], [19], [28] uses CPLEX and solves the Hottopixx models directly. Figure 1 summarizes the average elapsed time for each dataset. We can see from the figure that RCE is faster than CPLEX for $n \geq 1000$. In particular, RCE-SR is significantly faster than the other methods and its average elapsed time increases more slowly. RCE-DIR is faster than CPLEX-DIR, but its average elapsed time increases more rapidly than RCE-SR. The results suggest that RCE-SR should be used for the implementation of Hottopixx when dealing with large matrices.

B. Endmember Extraction Performance

Next, we examined the endmember extraction performance of EEHT on semi-real HSI datasets. The datasets were constructed from the Jasper Ridge and Samson HSI datasets. We extracted subimages in the manner described in Section V of [33]:

- Jasper Ridge consists of 100×100 pixels with 198 bands and contains 4 endmembers: Tree, Soil, Water, and Road.
- Samson consists of 95×95 pixels with 156 bands and contains 3 endmembers: Soil, Tree, and Water.

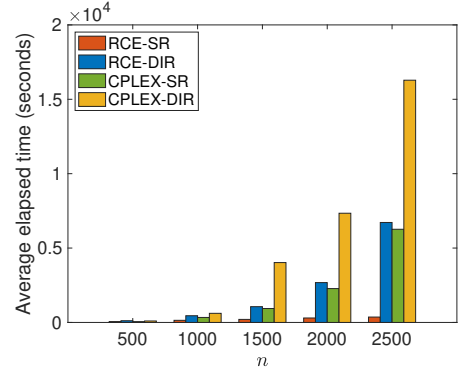


Fig. 1. Average elapsed time of four methods for five datasets.

The top of Figure 5 in Appendix F displays the RGB images of these datasets.

The endmember signatures in these regions were already identified in [33]. Using them as reference signatures, we constructed W, H and V as follows. Let A^{real} be the HSI matrix for a dataset, and $w_1^{\text{ref}}, \dots, w_r^{\text{ref}}$ be the reference signature vectors. Perform the following procedure:

- 1: Normalize all columns of A^{real} to have a unit L_1 norm.
- 2: For $i = 1, \dots, r$, find

$$j_i = \arg \min_{j=1, \dots, n} \text{MRSA}(a_j^{\text{real}}, w_i^{\text{ref}}),$$

and then construct $\mathcal{J} = \{j_1, \dots, j_r\}$.

- 3: Set $W = A^{\text{real}}(:, \mathcal{J})$.
- 4: Compute the optimal solution X of problem (4) by letting $(A, \mathcal{I}) = (A^{\text{real}}, \mathcal{J})$ in the problem. Set $X(:, \mathcal{J}) = I$ and then $H = X$.
- 5: Set $V = A^{\text{real}} - WH$.

We constructed two datasets using the W, H and V obtained above: dataset 1 from Jasper Ridge and dataset 2 from Samson. Each dataset contained 20 HSI matrices that were generated as follows: choose 20 equally spaced points between 0 and 1 as noise intensity levels ν ; and construct an HSI matrix $A = WH + (\nu/\|V\|_1) \cdot V$ for each ν . The HSI matrices A were of size 198×10000 with 4 endmembers for dataset 1 and of size 156×9025 with 3 endmembers for dataset 2. Note that $A = A^{\text{real}}$ holds if $\nu = \|V\|_1$, where $\|V\|_1 \approx 0.61$ for dataset 1 and $\|V\|_1 \approx 0.15$ for dataset 2.

We compared EEHT with six existing methods: MERIT, SPA, PSPA, ER, VCA, and SNPA. While MERIT, like EEHT, is a convex optimization-based method, the others are greedy methods. We developed MATLAB codes for SPA, PSPA and ER and used publicly available codes for MERIT, VCA, and SNPA, which were developed by the authors of [17], [29], [30]. We set the input parameters ζ and η of EEHT as $(\zeta, \eta) = (10, 100)$.

For a fair comparison with EEHT, we included the SVD-based dimensionality reduction, described in Section V, in MERIT: i.e., first compute the top- r truncated SVD $A_r = U_r \Sigma_r V_r^T$ of the input matrix A ; then run MERIT on $A' = \Sigma_r V_r^T$.

We ran EEHT and the six existing methods on datasets 1 and 2, and evaluated their performance by using the average

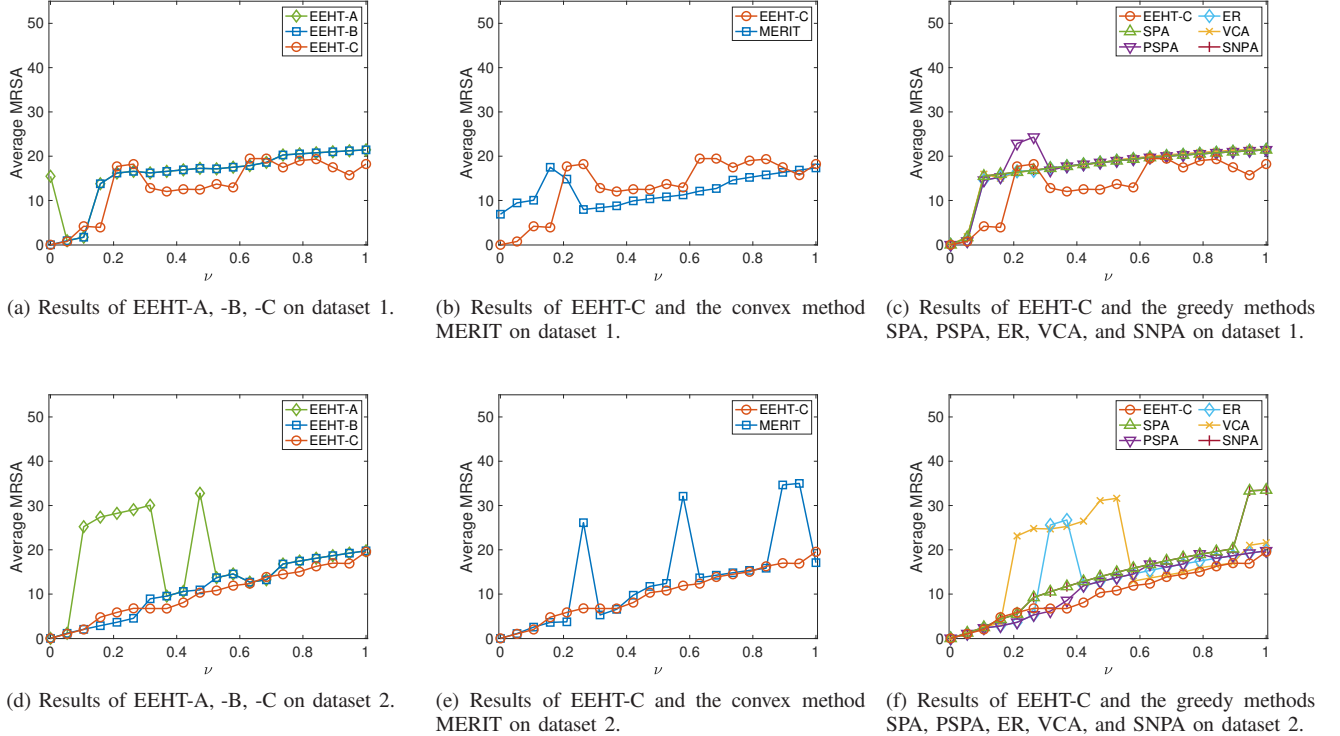


Fig. 2. Average MRSA value ($\times 10^2$) of EEHT and existing methods on dataset 1 (top) and dataset 2 (bottom).

MRSA given in (11). Regarding MERIT, it is necessary to fix the parameter λ of problem (6) and the parameter μ of the function ϕ_μ shown in (7) before it. In particular, the choice of λ affects its endmember extraction performance. We set μ to the default value of 10^{-5} , as suggested by the authors of [30]. We then set λ to $10^{-6}, 10^{-5}, \dots, 10^3$ and ran MERIT for each of these 10 values. For each λ value, we calculated the mean of the average MRSA values across all intensity levels ν . For dataset 1 (resp., dataset 2), the means were at their minimum when $\lambda = 10^2$ (resp., 10^{-1}). Therefore, we report the results of MERIT with $\lambda = 10^2$ for dataset 1 and $\lambda = 10^{-1}$ for dataset 2 in Figure 2.

The experiments were conducted by setting the parameters of the MERIT code [30] as follows. The value of λ can be specified using the `options.lambda` parameter, which we set as described above. Additionally, we set `options.backend` to `mex`. Default values were used for the remaining parameters.

Figure 2 plots the average MRSA values of the methods for datasets 1 and 2. We can see from the figure that, in most cases, EEHT-C achieved better average MRSA values than EEHT-A, -B, and the five greedy methods. This result suggests that using EEHT-C is preferable to EEHT-A and -B. EEHT-C achieved worse average MRSA values than MERIT for dataset 1, while it performed better than MERIT for dataset 2. For the 20 HSI matrices included in each dataset, the computation time of EEHT-A, -B and -C was approximately 30 minutes on average.

Remark 2: We ran FGNSR with an SVD-based dimensionality reduction on datasets 1 and 2. It took about two weeks

for each dataset. When running for multiple parameter values of λ , the computational time was excessively long. Thus, we did not conduct experiments on FGNSR.

Remark 3: Let us go back to the results of EEHT-A, -B, and -C on dataset 1 (top-left of Figure 2). One may wonder why EEHT-A took positive MRSA values at $\nu = 0$. Remark 4.1 of [28] predicts that this can happen if overlapping columns exist in the HSI matrices. Indeed, EEHT-A took a zero MRSA value for every endmember at $\nu = 0$ after eliminating the duplicate columns.

C. Hyperspectral Unmixing of Urban HSI

Finally, we conducted an experimental study on hyperspectral unmixing of the Urban HSI dataset. The image was taken over Copperas Cove, Texas, USA by the HYDICE sensor. It consists of 307×307 pixels with 210 bands from 400 nm to 2500 nm. Following the procedure in [32], [33], we removed dirty bands from the image. The resulting image had 162 clean bands. The experimental studies in [32], [33] showed that there are mainly 4-6 endmembers in the image. Following the settings used in [20], our experiments set the number of endmembers to 6: Asphalt, Grass, Tree, Roof 1, Roof 2 and Soil. These six endmember signatures were identified in [32]. We used them as reference signatures. The bottom of Figure 5 in Appendix F displays the RGB image of the Urban dataset.

We did not achieve satisfactory results for Urban by applying the methods that were tested on the semi-real HSI datasets described in Section VI-B. The estimated endmember signatures were not sufficiently close to the reference ones. Consequently, we conducted data-specific preprocessing aimed

at enhancing the endmember extraction performance of these methods. The preprocessing was based on a reasonable assumption that there are a number of pixels close to each pure pixel in an HSI. Indeed, this assumption holds in the case of the Urban dataset: see Table I that summarizes the number of pixels under an MRSA value of 0.05 relative to the reference signatures of the endmembers. Here, we shall say that pixels are *isolated* if there are almost no pixels close to them. Under this assumption, even if we remove isolated pixels, there would be little effect on the number of pure pixels. It is possible that some of the isolated pixels contain large amounts of noise, which would worsen the endmember extraction performance of the methods.

TABLE I
NUMBER OF PIXELS UNDER AN MRSA VALUE OF 0.05 RELATIVE TO THE REFERENCE SIGNATURES OF ENDMEMBERS FOR URBAN.

Asphalt	Grass	Tree	Roof 1	Roof 2	Soil
939	16,435	14,122	1,493	70	1,491

To find isolated pixels, we introduced the *neighborhood density* of each pixel, defined by

$$\rho(i; \phi) = \frac{1}{n} |\text{NH}(i; \phi)| \in [0, 1]$$

for the neighborhood of the i th pixel \mathbf{a}_i under an MRSA value of ϕ ,

$$\text{NH}(i; \phi) = \{j \in \mathcal{N} \mid \text{MRSA}(\mathbf{a}_i, \mathbf{a}_j) \leq \phi\},$$

and the total number n of pixels in an HSI. For Urban, we examined the neighborhood density ρ while varying ϕ . Figure 3 displays a histogram of ρ with a bin size of 0.01 when $\phi = 0.4$. We can see from the figure that there is a small peak in the low-density range from $\rho = 0.08$ to 0.09. In the experiments, we set $\phi = 0.4$ and removed all pixels \mathbf{a}_i satisfying $\rho(i; \phi) \leq \omega$ for a truncation parameter ω specified in advance. We ran the same methods as in Section VI-B for Urban while varying ω from 0 to 0.15.

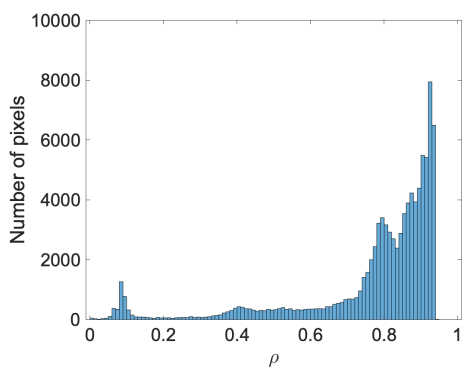


Fig. 3. Histogram of neighborhood density ρ versus the number of pixels for Urban with $\phi = 0.4$ (bin size 0.01).

First, let us examine the experiments on Urban with $\phi = 0.4$ and $\omega = 0.1$. Under these settings, there were 2955 pixels \mathbf{a}_i (3% for total number of pixels) satisfying $\rho(i; \phi) \leq \omega$. We removed all of those pixels. For EEHT, we set the input

parameters ζ and η as $(\zeta, \eta) = (50, 300)$. For MERIT, we used the same parameter values as in Section VI-B. We set λ to $10^{-6}, 10^{-5}, \dots, 10^3$. For each λ value, we ran MERIT and calculated the average MRSA values for six endmembers. The averages were at their minimum when $\lambda = 10^2$. Therefore, we reported the results of MERIT with $\lambda = 10^2$.

Table II summarizes the MRSA values for each endmember given in (10) and their averages given in (11). We can see from the table that the MRSA values of EEHT-C are smaller than those of the other methods, except in the case of Roof 2. Regarding computational time, EEHT-A, -B, and -C each took approximately 10 hours.

TABLE II
MRSA VALUES ($\times 10^2$) OF METHODS FOR URBAN WITH $\phi = 0.4$ AND $\omega = 0.1$. THE BEST SCORES ARE HIGHLIGHTED IN BOLD.

	Asphalt	Grass	Tree	Roof 1	Roof 2	Soil	Avg.
EEHT-A	11.2	15.7	44.2	12.5	17.1	10.4	18.5
EEHT-B	27.4	15.7	5.8	24.8	57.5	10.4	23.6
EEHT-C	9.2	5.7	3.4	7.1	18.9	3.2	7.9
MERIT	20.5	33.6	14.0	12.5	19.5	16.7	19.5
SPA	20.5	35.4	4.7	12.5	17.1	16.7	17.8
PSPA	20.5	6.4	4.7	12.5	17.1	16.7	13.0
ER	20.5	18.4	4.7	12.5	29.2	16.7	17.0
VCA	16.2	41.0	15.3	13.7	50.8	31.1	28.0
SNPA	12.7	27.0	4.7	12.5	44.6	16.7	19.7

To assess the effectiveness of EEHT-C further, we computed abundance maps by using the estimated endmember signatures and compared them with the ground truth derived from the reference signatures. Figure 6 in Appendix F displays them. We can see that the abundance maps obtained by EEHT-C are similar to those obtained by the reference signatures except Roof 2.

Next, let us examine the experiments on Urban with $\phi = 0.4$ and varying ω from 0 to 0.15 in 0.025 increments. Figure 4 plots the average MRSA values. We can see from the figure that EEHT-C performs better than the other methods in average MRSA, except when $\omega = 0.15$.

The average MRSA values of EEHT-C reach their minimum at $\omega = 0.1$. If ω is set to a large value, some of the pixels \mathbf{a}_i satisfying $\rho(i; \phi) \leq \omega$ are no longer isolated and may be close to pure pixels. Removing such pixels can affect the number of pure pixels in an HSI. To explore this, we set $\phi = 0.4$ and $\omega = 0.125$ and removed all pixels \mathbf{a}_i satisfying $\rho(i; \phi) \leq \omega$. At this setting, no pixels existed with an MRSA value of 0.05 relative to the reference signature of Roof 1. Accordingly, when $\omega \geq 0.125$, it was impossible for EEHT-C to identify pixels containing the spectral signature of Roof 1 with high purity. For this reason, the average MRSA values of EEHT-C increased.

As shown in Figure 4, the endmember extraction performance of the methods depends on the choice of ω . Details of the observation for choosing the value of ω are provided in Appendix E.

VII. CONCLUDING REMARKS

This study was motivated by the following question: although the theoretical results shown in [16], [28] suggest

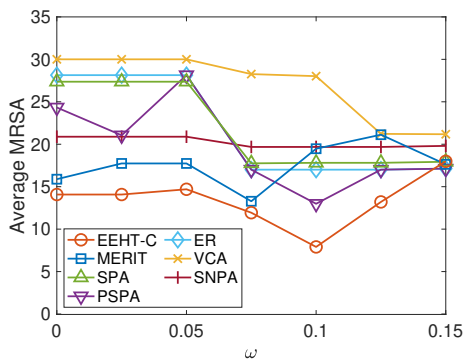


Fig. 4. Average MRSA values ($\times 10^2$) of methods for Urban with $\phi = 0.4$ and varying ω from 0 to 0.15 in 0.025 increments.

that Hottopixx methods are effective for endmember extraction problems, is this really true? Hottopixx methods require solving computationally expensive LP problems, called Hottopixx models, which makes them challenging to implement in practice. To address this issue, we developed an efficient and effective implementation of Hottopixx, EEHT, and found numerical evidence indicating that EEHT can estimate the endmember signatures of real HSIs with reasonable accuracy.

We close this paper with remarks on potential directions for future research. As we saw in Section VI-C, EEHT can be applied to endmember extraction of HSIs with around one hundred thousand pixels. However, its computational time is much longer than that of greedy methods, such as SPA and its refinements. In order to reduce it, we need to focus on the computational cost of RCE, whose bottleneck lies in computing the optimal solutions to problems $P(\mathcal{L}, \mathcal{L})$ and $D(\mathcal{L}, \mathcal{L})$ in step 2-1, since the problem size can be large. Augmented Lagrangian methods are often used for solving large-scale LPs; see [8], for instance. These methods may be of help in reducing the computational time required by EEHT.

REFERENCES

- [1] U. M. C. Araújo, B. T. C. Saldanha, R. K. H. Galvão, T. Yoneyama, H. C. Chame, and V. Visani. The successive projections algorithm for variable selection in spectroscopic multicomponent analysis. *Chemometrics and Intelligent Laboratory Systems*, 57(2):65–73, 2001.
- [2] S. Arora, R. Ge, R. Kannan, and A. Moitra. Computing a nonnegative matrix factorization – Provably. In *Proceedings of the 44th symposium on Theory of Computing (STOC)*, pages 145–162, 2012.
- [3] A. Ben-Tal and A. Nemirovski. *Lectures on Modern Convex Optimization*. SIAM, 2001.
- [4] D. Bertsimas and J. N. Tsitsiklis. *Introduction to Linear Optimization*. Athena Scientific, 1997.
- [5] J. M. Bioucas-Dias, A. Plaza, N. Dobigeon, M. Parente, Q. Du, P. Gader, and J. Chanussot. Hyperspectral unmixing overview: Geometrical, statistical, and sparse regression-based approaches. *IEEE Journal of Selected Topics in Applied Earth Observations and Remote Sensing*, 5(2):354–379, 2012.
- [6] V. Bittorf, B. Recht, C. Re, and J. A. Tropp. Factoring nonnegative matrices with linear programs. In *Proceedings of Advances in Neural Information Processing Systems 25 (NIPS)*, pages 1223–1231, 2012.
- [7] J. W. Boardman, F. A. Kruse, and R. O. Green. Mapping target signatures via partial unmixing of aviris data. In *Proceedings of JPL Airborne Earth Science Workshop*, pages 23–25, 1995.
- [8] S. Burer and D. Vandenbussche. Solving lift-and-project relaxations of binary integer programs. *SIAM Journal on Optimization*, 16(3):726–750, 2006.
- [9] T.-H. Chan, W.-K. Ma, A. Ambikapathi, and C.-Y. Chi. A simplex volume maximization framework for hyperspectral endmember extraction. *IEEE Transactions on Geoscience and Remote Sensing*, 49(11):4177–4193, 2011.
- [10] E. Elhamifar, G. Sapiro, and R. Vidal. See all by looking at a few: Sparse modeling for finding representative objects. In *Proceedings of IEEE Conference on Computer Vision and Pattern Recognition*, pages 1600–1608, 2012.
- [11] E. Esser, M. Möller, S. Osher, G. Sapiro, and J. Xin. A convex model for nonnegative matrix factorization and dimensionality reduction on physical space. *IEEE Transactions on Image Processing*, 21(7):3239–3252, 2012.
- [12] X. Fu, K. Huang, N. D. Sidiropoulos, and W.-K. Ma. Nonnegative matrix factorization for signal and data analytics: Identifiability, algorithms, and applications. *IEEE Signal Processing Magazine*, 36(2):59–80, 2019.
- [13] X. Fu and W.-K. Ma. Robustness analysis of structured matrix factorization via self-dictionary mixed-norm optimization. *IEEE Signal Processing Letters*, 23(1):60–64, 2016.
- [14] X. Fu, N. D. Sidiropoulos, and W.-K. Ma. Power spectra separation via structured matrix factorization. *IEEE Transactions on Signal Processing*, 64(17):4592–4605, 2016.
- [15] P. Ghamisi, N. Yokoya, J. Li, W. Liao, S. Liu, J. Plaza, B. Rasti, and A. Plaza. Advances in hyperspectral image and signal processing: A comprehensive overview of the state of the art. *IEEE Geoscience and Remote Sensing Magazine*, 5(4):37–78, 2018.
- [16] N. Gillis. Robustness analysis of Hottopixx, a linear programming model for factoring nonnegative matrices. *SIAM Journal on Matrix Analysis and Applications*, 34(3):1189–1212, 2013.
- [17] N. Gillis. Successive nonnegative projection algorithm for robust nonnegative blind source separation. *SIAM Journal on Imaging Sciences*, 7(2):1420–1450, 2014.
- [18] N. Gillis. *Nonnegative Matrix Factorization*. SIAM, 2020.
- [19] N. Gillis and R. Luce. Robust near-separable nonnegative matrix factorization using linear optimization. *Journal of Machine Learning Research*, 15:1249–1280, 2014.
- [20] N. Gillis and R. Luce. A fast gradient method for nonnegative sparse regression with self-dictionary. *IEEE Transactions on Image Processing*, 27(1):24–37, 2018.
- [21] N. Gillis and S. A. Vavasis. Fast and robust recursive algorithms for separable nonnegative matrix factorization. *IEEE Transactions on Pattern Analysis and Machine Intelligence*, 36(4):698–714, 2014.
- [22] N. Gillis and S. A. Vavasis. Semidefinite programming based preconditioning for more robust near-separable nonnegative matrix factorization. *SIAM Journal on Optimization*, 25(1):677–698, 2015.
- [23] M.-D. Iordache, J. M. Bioucas-Dias, and A. Plaza. Sparse unmixing of hyperspectral data. *IEEE Transactions on Geoscience and Remote Sensing*, 49(6):2014–2039, 2011.
- [24] M.-D. Iordache, J. M. Bioucas-Dias, and A. Plaza. Collaborative sparse regression for hyperspectral unmixing. *IEEE Transactions on Geoscience and Remote Sensing*, 52(1):341–354, 2014.
- [25] M.-D. Iordache, J. M. Bioucas-Dias, A. Plaza, and B. Somers. MUSIC-CSR: Hyperspectral unmixing via multiple signal classification and collaborative sparse regression. *IEEE Transactions on Geoscience and Remote Sensing*, 52(7):4364–4382, 2014.
- [26] W.-K. Ma, J. M. Bioucas-Dias, T.-H. Chan, N. Gillis, P. Gader, A. J. Plaza, A. Ambikapathi, and C.-Y. Chi. A signal processing perspective on hyperspectral unmixing. *IEEE Signal Processing Magazine*, 31(1):67–81, 2014.
- [27] T. Mizutani. Ellipsoidal rounding for nonnegative matrix factorization under noisy separability. *Journal of Machine Learning Research*, 15:1011–1039, 2014.
- [28] T. Mizutani. Refinement of Hottopixx method for nonnegative matrix factorization under noisy separability. *SIAM Journal on Matrix Analysis and Applications*, 43(3):1029–1057, 2022.
- [29] J. M. P. Nascimento and J. M. Bioucas-Dias. Vertex component analysis: A fast algorithm to unmix hyperspectral data. *IEEE Transactions on Geoscience and Remote Sensing*, 43(4):898–910, 2005.
- [30] T. Nguyen, X. Fu, and R. Wu. Memory-efficient convex optimization for self-dictionary separable nonnegative matrix factorization: A Frank-Wolfe approach. *IEEE Transactions on Signal Processing*, 70:3221–3236, 2022.
- [31] M. E. Winter. N-FINDR: an algorithm for fast autonomous spectral endmember determination in hyperspectral data. In *Proceedings of SPIE, Imaging Spectrometry V*, volume 3753, pages 266 – 275, 1999.
- [32] F. Zhu. Hyperspectral unmixing: Ground truth labeling, datasets, benchmark performances and survey. arXiv:1708.05125, 2017.

[33] F. Zhu, Y. Wang, B. Fan, S. Xiang, G. Meng, and C. Pan. Spectral unmixing via data-guided sparsity. *IEEE Transactions on Image Processing*, 23(12):5412–5427, 2014.

APPENDIX A
PROOF OF THEOREM 2

First, we will prove part (i) of Theorem 2 and then address part (ii).

Proof of part (i) of Theorem 2: First, we show that $\text{opt}(\text{H}(\mathcal{L}, \mathcal{L})) \geq \text{opt}(\text{H}(\mathcal{L}, \mathcal{N}))$ holds under condition (C1). The matrix $[X^*, \Gamma^*]$ belongs to $\mathcal{F}(\ell, n)$, and thus, it is a feasible solution to $\text{H}(\mathcal{L}, \mathcal{N})$. In addition, we obtain $\|A(\mathcal{L}) - A(\mathcal{L})X^*\|_1 = \text{opt}(\text{H}(\mathcal{L}, \mathcal{L}))$ by Theorem 1 (ii), and $\|A(\mathcal{N} \setminus \mathcal{L}) - A(\mathcal{L})\Gamma^*\|_1 \leq \text{opt}(\text{H}(\mathcal{L}, \mathcal{L}))$ by condition (C1) and Theorem 1 (i). Thus, the objective function value of $\text{H}(\mathcal{L}, \mathcal{N})$ at $[X^*, \Gamma^*]$ satisfies

$$\begin{aligned} \text{opt}(\text{H}(\mathcal{L}, \mathcal{N})) &\leq \|A\Pi - A(\mathcal{L})[X^*, \Gamma^*]\|_1 \\ &= \|[A(\mathcal{L}), A(\mathcal{N} \setminus \mathcal{L})] - A(\mathcal{L})[X^*, \Gamma^*]\|_1 \\ &= \|[A(\mathcal{L}) - A(\mathcal{L})X^*, A(\mathcal{N} \setminus \mathcal{L}) - A(\mathcal{L})\Gamma^*]\|_1 \\ &= \text{opt}(\text{H}(\mathcal{L}, \mathcal{L})). \end{aligned}$$

Next, we show the reverse inequality. Let $\hat{X}^* = [\hat{x}_1^*, \dots, \hat{x}_n^*]$ denote the optimal solution of $\text{H}(\mathcal{L}, \mathcal{N})$. We find that

$$\begin{aligned} \text{opt}(\text{H}(\mathcal{L}, \mathcal{N})) &= \|A\Pi - A(\mathcal{L})\hat{X}^*\|_1 \\ &= \|[A(\mathcal{L}), A(\mathcal{N} \setminus \mathcal{L})] - A(\mathcal{L})\hat{X}^*\|_1 \\ &\geq \|[A(\mathcal{L}) - A(\mathcal{L})[\hat{x}_1^*, \dots, \hat{x}_\ell^*]]\|_1 \\ &\geq \text{opt}(\text{H}(\mathcal{L}, \mathcal{L})). \end{aligned}$$

The last inequality comes from that the matrix $[\hat{x}_1^*, \dots, \hat{x}_\ell^*]$ belongs to $\mathcal{F}(\ell, \ell)$ and is, therefore, a feasible solution to $\text{H}(\mathcal{L}, \mathcal{L})$. The two inequalities we showed above yield

$$\text{opt}(\text{H}(\mathcal{L}, \mathcal{L})) = \text{opt}(\text{H}(\mathcal{L}, \mathcal{N})) = \|A\Pi - A(\mathcal{L})[X^*, \Gamma^*]\|_1.$$

We conclude that $\text{opt}(\text{H}(\mathcal{L}, \mathcal{L})) = \text{opt}(\text{H}(\mathcal{L}, \mathcal{N}))$ and the matrix $[X^*, \Gamma^*]$ is the optimal solution to $\text{H}(\mathcal{L}, \mathcal{N})$. ■

Next, we prove part (ii) of Theorem 2. To do so, we need Lemmas 2 and 3.

- *Lemma 2:* Let α^* be the optimal solution of $\text{P}(\mathcal{L}, \mathcal{L})$. If α^* satisfies condition (C1), then α can be constructed from α^* such that α is a feasible solution to $\text{P}(\mathcal{N}, \mathcal{N})$, and the objective function value of $\text{P}(\mathcal{N}, \mathcal{N})$ at α is $\text{opt}(\text{P}(\mathcal{L}, \mathcal{L}))$.
- *Lemma 3:* Let β^* be the optimal solution of $\text{D}(\mathcal{L}, \mathcal{L})$. If β^* satisfies condition (C2), then β can be constructed from β^* such that β is a feasible solution of $\text{D}(\mathcal{N}, \mathcal{N})$, and the objective function value of $\text{D}(\mathcal{N}, \mathcal{N})$ at β is $\text{opt}(\text{D}(\mathcal{L}, \mathcal{L}))$.

Theorem 1 (i) tells us that $\text{opt}(\text{P}(\mathcal{L}, \mathcal{L})) = \text{opt}(\text{D}(\mathcal{L}, \mathcal{L}))$. Accordingly, as we reviewed in Section II-B, the weak duality theorem implies that α and β are optimal solutions to $\text{P}(\mathcal{N}, \mathcal{N})$ and $\text{D}(\mathcal{N}, \mathcal{N})$, respectively. Furthermore, it means that $\text{opt}(\text{P}(\mathcal{N}, \mathcal{N})) = \text{opt}(\text{P}(\mathcal{L}, \mathcal{L}))$. As a result, using parts (i) and (ii) of Theorem 1, we can establish part (ii) of Theorem 2.

Here, we give formal descriptions of Lemmas 2 and 3 and then prove them.

Lemma 2: Let $\mathcal{L} \subset \mathcal{N}$. Let $\alpha^* = (X^*, F^*, G^*, u^*)$ be the optimal solution of $\text{P}(\mathcal{L}, \mathcal{L})$. Assume that condition (C1) holds. By letting $\Gamma^* = [\gamma_j^* : j \in \mathcal{N} \setminus \mathcal{L}]$ for the optimal solution γ_j^* of $\text{R}_j(\mathcal{L}, X^*)$ and letting Π be a permutation matrix of size n satisfying $A\Pi = [A(\mathcal{L}), A(\mathcal{N} \setminus \mathcal{L})]$, construct $\alpha = (X, F, G, u) \in \mathbb{R}^{n \times n} \times \mathbb{R}^{d \times n} \times \mathbb{R}^{d \times n} \times \mathbb{R}$ as follows:

$$X = \Pi \begin{bmatrix} X^* & \Gamma^* \\ O & O \end{bmatrix} \Pi^\top, \quad F = R^+, \quad G = R^- \quad \text{and} \quad u = \|R\|_1$$

where $R = A - AX$ for X as constructed above. Then, the following hold.

- α is a feasible solution to $\text{P}(\mathcal{N}, \mathcal{N})$.
- The objective function value of $\text{P}(\mathcal{N}, \mathcal{N})$ at α is $\text{opt}(\text{P}(\mathcal{L}, \mathcal{L}))$, i.e., $u = \text{opt}(\text{P}(\mathcal{L}, \mathcal{L}))$.

Proof: As a simplification, we can write $X = \Pi\hat{X}\Pi^\top$ for X above by letting

$$\hat{X} = \begin{bmatrix} X^* & \Gamma^* \\ O & O \end{bmatrix}.$$

Part (i) It is sufficient to prove that α satisfies the first, second, and fifth constraints of $\text{P}(\mathcal{N}, \mathcal{N})$, since $F = R^+ \geq O$ and $G = R^- \geq O$. Let us look at the first constraint. Since R , F and G are constructed as $R = A - AX$, $F = R^+$ and $G = R^-$, we have

$$A - AX = R = R^+ - R^- = F - G.$$

Next, let us look at the second constraint. Equality (1) tells us that

$$u = \|R\|_1 = \max_{j=1, \dots, n} \sum_{i=1}^d R^+(i, j) + R^-(i, j).$$

This implies that $\sum_{i=1}^d F(i, j) + G(i, j) \leq u$ holds for $j = 1, \dots, n$. Finally, let us look at the fifth constraint. Since $X^* \in \mathcal{F}(\ell, \ell)$ and $\mathbf{0} \leq \gamma_j^* \leq \text{diag}(X^*)$, we see that $\hat{X} \in \mathcal{F}(n, n)$. Additionally, since X is constructed as $X = \Pi\hat{X}\Pi^\top$, the (i, j) th entry of X is given by $\hat{X}(\sigma(i), \sigma(j))$ for some permutation σ of size n . Hence, $X \in \mathcal{F}(n, n)$. Thus, the desired result follows.

Part (ii) The objective function value of $\text{P}(\mathcal{N}, \mathcal{N})$ at α can be rewritten as

$$u = \|R\|_1 = \|A - AX\|_1 = \|A\Pi - A\Pi\hat{X}\|_1.$$

In light of the relation $A\Pi = [A(\mathcal{L}), A(\mathcal{N} \setminus \mathcal{L})]$, it can be further expressed as

$$\|A\Pi - A\Pi\hat{X}\|_1 = \|[S, T]\|_1$$

for $S = A(\mathcal{L}) - A(\mathcal{L})X^*$ and $T = A(\mathcal{N} \setminus \mathcal{L}) - A(\mathcal{L})\Gamma^*$. It follows from parts (i) and (ii) of Theorem 1 that $\text{opt}(\text{P}(\mathcal{L}, \mathcal{L})) = \text{opt}(\text{H}(\mathcal{L}, \mathcal{L})) = \|A(\mathcal{L}) - A(\mathcal{L})X^*\|_1 = \|S\|_1$. It follows from condition (C1) that $\|T\|_1 = \|A(\mathcal{N} \setminus \mathcal{L}) - A(\mathcal{L})\Gamma^*\|_1 \leq \text{opt}(\text{P}(\mathcal{L}, \mathcal{L}))$. Consequently, we obtain $u = \text{opt}(\text{P}(\mathcal{L}, \mathcal{L}))$. ■

Lemma 3: Let $\mathcal{L} \subset \mathcal{N}$. Let $\beta^* = (Y^*, Z^*, \mathbf{s}^*, \mathbf{t}^*, v^*)$ be the optimal solution of $\text{D}(\mathcal{L}, \mathcal{L})$. Assume that condition (C2) holds. By letting Π be a permutation matrix of size n satisfying

$A\Pi = [A(\mathcal{L}), A(\mathcal{N} \setminus \mathcal{L})]$, and $\Delta = (Y^*)^\top A(\mathcal{N} \setminus \mathcal{L})$, construct $\beta = (Y, Z, \mathbf{s}, \mathbf{t}, v) \in \mathbb{R}^{d \times n} \times \mathbb{R}^{n \times n} \times \mathbb{R}^n \times \mathbb{R}^n \times \mathbb{R}$ as follows:

$$Y = [Y^*, O] \Pi^\top, \quad Z = \Pi \begin{bmatrix} Z^* & \Delta^+ \\ O & O \end{bmatrix} \Pi^\top, \quad \mathbf{s} = \Pi \begin{bmatrix} \mathbf{s}^* \\ \mathbf{0} \end{bmatrix},$$

$$\mathbf{t} = \Pi \begin{bmatrix} \mathbf{t}^* \\ \mathbf{0} \end{bmatrix} \quad \text{and } v = v^*.$$

Then, the following hold.

- (i) β is a feasible solution to $D(\mathcal{N}, \mathcal{N})$.
- (ii) The objective function value of $D(\mathcal{N}, \mathcal{N})$ at β is $\text{opt}(D(\mathcal{L}, \mathcal{L}))$.

Proof: The proof uses the following relation. Let $\mathbf{a} \in \mathbb{R}^n$ and $P \in \mathbb{R}^{n \times n}$ be a permutation matrix. Then, a straightforward calculation gives

$$\text{diag}(P\mathbf{a}) = P\text{diag}(\mathbf{a})P^\top. \quad (12)$$

As a simplification, we can write $Y = \hat{Y}\Pi^\top, Z = \Pi\hat{Z}\Pi^\top, \mathbf{s} = \Pi\hat{\mathbf{s}}$ and $\mathbf{t} = \Pi\hat{\mathbf{t}}$ for $\hat{Y}, \hat{Z}, \hat{\mathbf{s}}$ and $\hat{\mathbf{t}}$ above by letting

$$\hat{Y} = [Y^*, O], \quad \hat{Z} = \begin{bmatrix} Z^* & \Delta^+ \\ O & O \end{bmatrix}, \quad \hat{\mathbf{s}} = \begin{bmatrix} \mathbf{s}^* \\ \mathbf{0} \end{bmatrix} \quad \text{and } \hat{\mathbf{t}} = \begin{bmatrix} \mathbf{t}^* \\ \mathbf{0} \end{bmatrix}.$$

Part (i) It is sufficient to prove that β satisfies the first and the second constraints of $D(\mathcal{N}, \mathcal{N})$, since, obviously, it satisfies the other constraints. First, look at the second constraint. We find that β satisfies the second constraint of $D(\mathcal{N}, \mathcal{N})$ if and only if β^* satisfies that of $D(\mathcal{L}, \mathcal{L})$. Indeed,

$$\begin{aligned} & -J \cdot \text{diag}(\mathbf{s}) \leq Y \leq J \cdot \text{diag}(\mathbf{s}) \\ \Leftrightarrow & -J \cdot \text{diag}(\Pi\hat{\mathbf{s}}) \leq \hat{Y}\Pi^\top \leq J \cdot \text{diag}(\Pi\hat{\mathbf{s}}) \\ \Leftrightarrow & -J\Pi \cdot \text{diag}(\hat{\mathbf{s}}) \cdot \Pi^\top \leq \hat{Y}\Pi^\top \leq J\Pi \cdot \text{diag}(\hat{\mathbf{s}}) \cdot \Pi^\top \quad (\text{by (12)}) \\ \Leftrightarrow & -J \cdot \text{diag}(\hat{\mathbf{s}}) \leq \hat{Y} \leq J \cdot \text{diag}(\hat{\mathbf{s}}) \\ \Leftrightarrow & -J \cdot \text{diag}(\mathbf{s}^*) \leq Y^* \leq J \cdot \text{diag}(\mathbf{s}^*). \end{aligned}$$

Next, look at the first constraint. By plugging in β on the left-hand side of the constraint, we get the following matrix $M \in \mathbb{R}^{n \times n}$:

$$M = A^\top Y + vI - \text{diag}(\mathbf{t}) - Z^\top + \text{diag}(Z^\top \mathbf{1}).$$

Then, we rewrite M as

$$\begin{aligned} M &= A^\top \hat{Y}\Pi^\top + v^*I - \Pi \cdot \text{diag}(\hat{\mathbf{t}}) \cdot \Pi^\top - \Pi\hat{Z}^\top\Pi^\top \\ &\quad + \Pi \cdot \text{diag}(\hat{Z}^\top \mathbf{1}) \cdot \Pi^\top \quad (\text{by (12)}) \\ &= \Pi(A\Pi)^\top \hat{Y}\Pi^\top + v^*I - \Pi \cdot \text{diag}(\hat{\mathbf{t}}) \cdot \Pi^\top - \Pi\hat{Z}^\top\Pi^\top \\ &\quad + \Pi \cdot \text{diag}(\hat{Z}^\top \mathbf{1}) \cdot \Pi^\top, \end{aligned}$$

which yields

$$\Pi^\top M \Pi = (A\Pi)^\top \hat{Y} + v^*I - \text{diag}(\hat{\mathbf{t}}) - \hat{Z}^\top + \text{diag}(\hat{Z}^\top \mathbf{1}).$$

Here,

$$\begin{aligned} (A\Pi)^\top \hat{Y} &= \begin{bmatrix} A(\mathcal{L})^\top Y^* & O \\ A(\mathcal{N} \setminus \mathcal{L})^\top Y^* & O \end{bmatrix}, \\ \text{diag}(\hat{\mathbf{t}}) &= \begin{bmatrix} \text{diag}(\mathbf{t}^*) & O \\ O & O \end{bmatrix}, \\ \hat{Z}^\top &= \begin{bmatrix} (Z^*)^\top & O \\ (\Delta^+)^\top & O \end{bmatrix}, \\ \text{diag}(\hat{Z}^\top \mathbf{1}) &= \begin{bmatrix} \text{diag}((Z^*)^\top \mathbf{1}) & O \\ O & \text{diag}((\Delta^+)^\top \mathbf{1}) \end{bmatrix}. \end{aligned}$$

We set $\tilde{M} = \Pi^\top M \Pi$ and partition \tilde{M} into four blocks $\tilde{M}_{11} \in \mathbb{R}^{\ell \times \ell}, \tilde{M}_{12} \in \mathbb{R}^{\ell \times (n-\ell)}, \tilde{M}_{21} \in \mathbb{R}^{(n-\ell) \times \ell}$ and $\tilde{M}_{22} \in \mathbb{R}^{(n-\ell) \times (n-\ell)}$ in the following manner:

$$\tilde{M} = \begin{bmatrix} \tilde{M}_{11} & \tilde{M}_{12} \\ \tilde{M}_{21} & \tilde{M}_{22} \end{bmatrix}$$

where each block is given as

$$\begin{aligned} \tilde{M}_{11} &= A(\mathcal{L})^\top Y^* + v^*I - \text{diag}(\mathbf{t}^*) - (Z^*)^\top + \text{diag}((Z^*)^\top \mathbf{1}), \\ \tilde{M}_{12} &= O, \\ \tilde{M}_{21} &= A(\mathcal{N} \setminus \mathcal{L})^\top Y^* - (\Delta^+)^\top, \\ \tilde{M}_{22} &= v^*I + \text{diag}((\Delta^+)^\top \mathbf{1}). \end{aligned}$$

We observe the following: $\tilde{M}_{11} \leq O$ since β^* satisfies the first constraint of $D(\mathcal{L}, \mathcal{L})$; $\tilde{M}_{21} \leq O$ since

$$\tilde{M}_{21} = A(\mathcal{N} \setminus \mathcal{L})^\top Y^* - (\Delta^+)^\top = \Delta^\top - (\Delta^+)^\top \leq O;$$

and, $\tilde{M}_{22} \leq O$ since

$$\begin{aligned} \tilde{M}_{22} &= v^*I + \text{diag}((\Delta^+)^\top \mathbf{1}) \\ &= \text{diag}(v^* + \mathbf{1}^\top \Delta^+(\cdot, 1), \dots, v^* + \mathbf{1}^\top \Delta^+(\cdot, n-\ell)) \\ &\leq O \quad (\text{by condition (C2)}). \end{aligned}$$

Accordingly, $\tilde{M} = \Pi^\top M \Pi \leq O \Leftrightarrow M \leq O$, which means that β satisfies the first constraint of $D(\mathcal{N}, \mathcal{N})$. Consequently, we obtain the desired result.

Part (ii) By a straightforward calculation, we find that

$$\begin{aligned} \langle A, Y \rangle + rv - \mathbf{1}^\top \mathbf{t} &= \langle A\Pi, Y\Pi \rangle + rv - \mathbf{1}^\top \mathbf{t} \\ &= \langle [A(\mathcal{L}), A(\mathcal{N} \setminus \mathcal{L})], [Y^*, O] \rangle + rv^* \\ &\quad - \mathbf{1}^\top \Pi \hat{\mathbf{t}} \\ &= \langle A(\mathcal{L}), Y^* \rangle + rv^* - \mathbf{1}^\top \mathbf{t}^* \\ &= \text{opt}(D(\mathcal{L}, \mathcal{L})). \end{aligned}$$

Now, we are ready to prove part (ii) of Theorem 2. ■

Proof of part (ii) of Theorem 2: Let α and β be as constructed in Lemmas 2 and 3. From the lemmas and Theorem 1 (i), we find that α and β are feasible solutions to $P(\mathcal{N}, \mathcal{N})$ and $D(\mathcal{N}, \mathcal{N})$ and the objective function value of $P(\mathcal{N}, \mathcal{N})$ at α is equal to that of $D(\mathcal{N}, \mathcal{N})$ at β . Thus, the weak duality theorem implies that α and β are optimal solutions to $P(\mathcal{N}, \mathcal{N})$ and $D(\mathcal{N}, \mathcal{N})$. Furthermore, this means that $\text{opt}(P(\mathcal{L}, \mathcal{L})) = \text{opt}(P(\mathcal{N}, \mathcal{N}))$. Consequently, it follows from parts (i) and (ii) of Theorem 1 that $\text{opt}(H(\mathcal{L}, \mathcal{L})) = \text{opt}(H(\mathcal{N}, \mathcal{N}))$ holds and X of α is the optimal solution to $H(\mathcal{N}, \mathcal{N})$. ■

APPENDIX B

CLUSTER CONSTRUCTION IN STEP 2-1 OF ALGORITHM 1

Here, we describe the notation for method of constructing a cluster \mathcal{S}_ℓ in step 2-1 of Algorithm 1. We choose a column \mathbf{a}_i of A and sort the columns $\mathbf{a}_1, \dots, \mathbf{a}_n$ of A by their distance to \mathbf{a}_i in ascending order so that

$$\|\mathbf{a}_i - \mathbf{a}_{u_1}\|_1 \leq \|\mathbf{a}_i - \mathbf{a}_{u_2}\|_1 \leq \dots \leq \|\mathbf{a}_i - \mathbf{a}_{u_{n-1}}\|_1$$

where $\{i, u_1, \dots, u_{n-1}\} = \mathcal{N}$. We then construct

$$\Omega_i = \{\{i\}, \{i, u_1\}, \{i, u_1, u_2\}, \dots, \{i, u_1, u_2, \dots, u_{n-1}\}\}.$$

Let $\mathcal{S} \in \Omega_i$ and $\mathbf{p} \in \mathbb{R}_+^n$. We regard \mathbf{p} as a point list for \mathcal{S} and define the score of \mathcal{S} based on the point list \mathbf{p} as follows:

$$\text{score}(\mathcal{S}, \mathbf{p}) = \sum_{u \in \mathcal{S}} \mathbf{p}(u).$$

Additionally, we define the diameter of \mathcal{S} in Ω_i by

$$\text{diam}(\mathcal{S}) = \max_{u \in \mathcal{S}} \|\mathbf{a}_i - \mathbf{a}_u\|_1.$$

Now, let $\Psi(\mathbf{p}) = \Psi_1(\mathbf{p}) \cup \dots \cup \Psi_n(\mathbf{p})$ where

$$\Psi_i(\mathbf{p}) = \left\{ \mathcal{S} \in \Omega_i \mid \text{score}(\mathcal{S}, \mathbf{p}) > \frac{r}{r+1} \right\}.$$

Step 2-1 of Algorithm 1 constructs \mathcal{S}_ℓ as follows:

$$\mathcal{S}_\ell = \arg \min_{\mathcal{S} \in \Psi(\mathbf{p}_\ell)} \text{diam}(\mathcal{S}).$$

APPENDIX C PROOF OF THEOREM 1

Proof: Let (X^*, F^*, G^*, u^*) be the optimal solution of $\text{P}(\mathcal{L}, \mathcal{M})$. Then, X^* is a feasible solution of $\text{H}(\mathcal{L}, \mathcal{M})$. Thus, we get $\text{opt}(\text{H}(\mathcal{L}, \mathcal{M})) \leq \|A(\mathcal{M})\Pi - A(\mathcal{L})X^*\|_1$. Furthermore, taking into account that (X^*, F^*, G^*, u^*) satisfies all constraints of $\text{P}(\mathcal{L}, \mathcal{M})$, we find that

$$\begin{aligned} \|A(\mathcal{M})\Pi - A(\mathcal{L})X^*\|_1 &= \|F^* - G^*\|_1 \\ &= \max_{j=1, \dots, m} \|F^*(:, j) - G^*(:, j)\|_1 \\ &\leq \max_{j=1, \dots, m} \|F^*(:, j)\|_1 + \|G^*(:, j)\|_1 \\ &= \max_{j=1, \dots, m} \sum_{i=1}^d F^*(i, j) + G^*(i, j) \\ &\leq u^* = \text{opt}(\text{P}(\mathcal{L}, \mathcal{M})). \end{aligned}$$

Accordingly,

$$\text{opt}(\text{H}(\mathcal{L}, \mathcal{M})) \leq \|A(\mathcal{M})\Pi - A(\mathcal{L})X^*\|_1 \leq \text{opt}(\text{P}(\mathcal{L}, \mathcal{M})). \quad (13)$$

Let \hat{X}^* be the optimal solution of $\text{H}(\mathcal{L}, \mathcal{M})$, and let us use it to construct $R = A(\mathcal{M})\Pi - A(\mathcal{L})\hat{X}^*$. Note that R satisfies the relation $\|R\|_1 = \text{opt}(\text{H}(\mathcal{L}, \mathcal{M}))$, which will be used below. We show that $(\hat{X}^*, R^+, R^-, \|R\|_1)$ is a feasible solution of $\text{P}(\mathcal{L}, \mathcal{M})$. Obviously, it satisfies all the constraints except the second one. Here, recall equality (1) shown in Section II-A. For the second constraint, this equality implies that

$$\sum_{i=1}^d R^+(i, j) + R^-(i, j) \leq \|R\|_1.$$

Accordingly,

$$\text{opt}(\text{H}(\mathcal{L}, \mathcal{M})) = \|R\|_1 \geq \text{opt}(\text{P}(\mathcal{L}, \mathcal{M})). \quad (14)$$

In addition, as explained just before this theorem, the duality theorem ensures

$$\text{opt}(\text{P}(\mathcal{L}, \mathcal{M})) = \text{opt}(\text{D}(\mathcal{L}, \mathcal{M})). \quad (15)$$

From (13), (14) and (15), we obtain the equalities,

$$\begin{aligned} \text{opt}(\text{P}(\mathcal{L}, \mathcal{M})) &= \text{opt}(\text{D}(\mathcal{L}, \mathcal{M})) = \text{opt}(\text{H}(\mathcal{L}, \mathcal{M})) \\ &= \|A(\mathcal{M})\Pi - A(\mathcal{L})X^*\|_1 = \|R\|_1. \end{aligned}$$

As shown above, X^* and $(\hat{X}^*, R^+, R^-, \|R\|_1)$ are feasible solutions of $\text{H}(\mathcal{L}, \mathcal{M})$ and $\text{P}(\mathcal{L}, \mathcal{M})$, respectively. Hence, this completes the proof of parts (i)-(iii). ■

APPENDIX D PROOF OF LEMMA 1

Proof: We plug in the optimal solution of $\text{D}(\mathcal{L}, \mathcal{L})$ for the first constraint and then express the resulting inequality as $M \leq O$ by letting

$$M = A(\mathcal{L})^\top Y^* + v^* I - \text{diag}(\mathbf{t}^*) - (Z^*)^\top + \text{diag}((Z^*)^\top \mathbf{1}).$$

The trace of M is given as

$$\text{tr}(M) = \langle A(\mathcal{L}), Y^* \rangle + \ell v^* - \mathbf{1}^\top \mathbf{t}^* + \sum_{i \neq j} Z^*(i, j).$$

Here, the sum of $Z^*(i, j)$ runs over all pairs (i, j) except $i = j$. Let $c = \langle A(\mathcal{L}), Y^* \rangle + \ell v^* - \mathbf{1}^\top \mathbf{t}^*$. Then, $\text{opt}(\text{D}(\mathcal{L}, \mathcal{L})) - c = (r - \ell)v^*$. We use this relation to prove the lemma. We have $c \leq 0$, since

$$c = \langle A(\mathcal{L}), Y^* \rangle + \ell v^* - \mathbf{1}^\top \mathbf{t}^* = \text{tr}(M) - \sum_{i \neq j} Z^*(i, j) \leq 0$$

by $M \leq O$ and $Z^* \geq O$. We also have $\text{opt}(\text{D}(\mathcal{L}, \mathcal{L})) \geq 0$. Indeed, $\text{opt}(\text{D}(\mathcal{L}, \mathcal{L})) = \text{opt}(\text{H}(\mathcal{L}, \mathcal{L}))$ by Theorem 1 (i), and $\text{opt}(\text{H}(\mathcal{L}, \mathcal{L})) \geq 0$, since the objective function value of $\text{H}(\mathcal{L}, \mathcal{L})$ always takes a nonnegative value. We thus get

$$\text{opt}(\text{D}(\mathcal{L}, \mathcal{L})) - c \geq 0 \Leftrightarrow (r - \ell)v^* \geq 0.$$

This implies that $v^* \leq 0$, since \mathcal{L} is chosen to be $\ell \geq r \Leftrightarrow r - \ell \leq 0$. ■

APPENDIX E CHOOSING THE VALUE OF ω

Our data-specific preprocessing for the Urban HSI dataset requires us to choose two parameters ϕ and ω . In particular, as shown in Figure 4, the endmember extraction performance of the methods depends on the choice of ω . When drawing the histogram of density ρ versus the number of pixels while varying ϕ from 0.45 to 0.6 in 0.05 increments, as in the case where $\phi = 0.4$, a small peak appeared in a low-density range. Therefore, on the basis of the experimental results for $\phi = 0.4$, we can describe the criteria for choosing ω when ϕ is between 0.45 and 0.6 as follows.

- (1) When drawing the histogram of density ρ , a peak in a low-density range should be truncated by ω .
- (2) The value of ω should be small to prevent pixels close to pure pixels from being removed.

We chose ω by following criteria (1) and (2) and ran EEHT-C and six existing methods on Urban. Table III summarizes the average MRSA values. We see that the average MRSA values of EEHT-C are nearly unchanged for ϕ from 0.4 to 0.6. These results show that criteria (1) and (2) for choosing ω can yield consistent endmember extraction results for EEHT-C on Urban when ϕ belongs to this range.

TABLE III
 AVERAGE MRSA VALUES ($\times 10^2$) OF METHODS RUN ON URBAN WHILE VARYING ϕ AND USING CRITERIA (1) AND (2) FOR THE CHOICE OF ω . THE BEST SCORES ARE HIGHLIGHTED IN BOLD.

ϕ	ω	EEHT-C	MERIT	SPA	PSPA	ER	VCA	SNPA
0.40	0.10	7.9	19.5	17.8	13.0	17.0	28.0	19.7
0.45	0.15	8.4	17.0	17.8	17.0	17.0	28.3	19.7
0.50	0.30	9.3	17.0	17.8	17.0	17.0	28.3	19.7
0.55	0.45	8.2	11.9	17.8	17.0	17.0	28.0	19.7
0.60	0.60	8.2	17.0	17.8	17.0	17.0	28.3	19.7

APPENDIX F FIGURES

Figure 5 displays the RGB images of three datasets: Jasper Ridge, Samson, and Urban. Figure 6 presents the ground truth and abundance maps obtained by EEHT-C and six existing methods for the Urban dataset with $\phi = 0.4$ and $\omega = 0.1$. The ground truth was derived by using the reference signatures.



Fig. 5. RGB images of Jasper Ridge (top-left), Samson (top-right), and Urban (bottom).

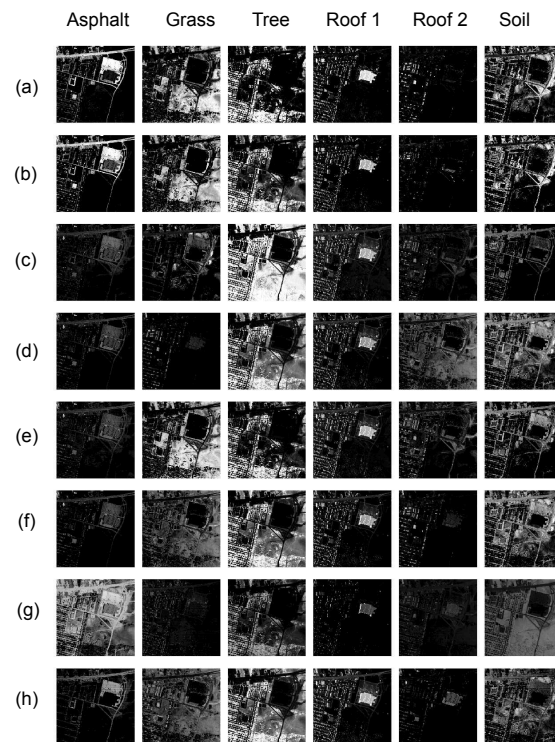


Fig. 6. Ground truth and abundance maps obtained by the methods for Urban with $\phi = 0.4$ and $\omega = 0.1$: (a) ground truth obtained by using the reference signatures, (b) EEHT-C, (c) MERIT, (d) SPA, (e) PSPA, (f) ER, (g) VCA, and (h) SNPA.